



EPA Public Access

Author manuscript

Atmos Meas Tech. Author manuscript; available in PMC 2021 May 19.

About author manuscripts

Submit a manuscript

Published in final edited form as:

Atmos Meas Tech. 2020 May 19; 13(5): . doi:10.5194/amt-13-2523-2020.

Assessment of NO₂ observations during DISCOVER-AQ and KORUS-AQ field campaigns

Sungyeon Choi^{1,2}, Lok N. Lamsal^{1,3}, Melanie Follette-Cook^{1,4}, Joanna Joiner¹, Nickolay A. Krotkov¹, William H. Swartz⁵, Kenneth E. Pickering^{1,6}, Christopher P. Loughner⁷, Wyatt Appel⁸, Gabriele Pfister⁹, Pablo E. Saide¹⁰, Ronald C. Cohen¹¹, Andrew J. Weinheimer⁹, Jay R. Herman^{1,12}

¹NASA Goddard Space Flight Center, Greenbelt, MD 20771, USA

²Science Systems and Applications, Inc., Lanham, MD 20706, USA

³Universities Space Research Association, Columbia, MD 21046, USA

⁴Goddard Earth Sciences Technology and Research, Morgan State University, Baltimore, MD 20251, USA

⁵Johns Hopkins University, Applied Physics Laboratory, Laurel, MD 20723, USA

⁶Department of Atmospheric and Oceanic Science, University of Maryland, College Park, MD 20742, USA

⁷NOAA Air Resources Laboratory, College Park, MD 20740, USA

⁸Environmental Protection Agency, Research Triangle Park, NC 27709, USA

⁹National Center for Atmospheric Research, Boulder, CO 80301, USA

¹⁰Department of Atmospheric and Oceanic Sciences, and Institute of the Environment and Sustainability, University of California, Los Angeles, CA 90095, USA

¹¹Department of Chemistry and Department of Earth and Planetary Science, University of California, Berkeley, CA 94720, USA

This work is distributed under the Creative Commons Attribution 4.0 License.

Correspondence: Sungyeon Choi (sungyeon.choi@nasa.gov).

Author contributions.

SC, LL, JJ, NAK, MFC, WHS, and KEP designed the data analysis. CPL, WA, GP, and PES provided the model simulations. RCC and AJW provided the airborne in situ measurements. JRH provided the ground-based Pandora measurements. SC, LL, MFC, WHS, CPL, WA, and PES wrote the paper with comments from all coauthors.

Competing interests.

The authors declare that they have no conflict of interest.

Data availability.

Airborne, ground-based, and Pandora NO₂ data gathered during the DISCOVER-AQ and KORUS-AQ campaigns are available at the NASA Langley campaign data web archive (<https://doi.org/10.5067/AIRCRAFT/DISCOVER-AQ/AEROSOL-TRACEGAS>, DISCOVER-AQ Science Team, 2014; <https://doi.org/10.5067/Suborbital/KORUS-AQ/DATA01>, KORUS-AQ Science Team, 2018). OMI NO₂ Standard Product (SP) data are available at the NASA Goddard Earth Sciences Data and Information Services Center (GES DISC) (<https://doi.org/10.5067/Aura/OMI/DATA2017>, Krotkov et al., 2019).

Review statement.

This paper was edited by Michel Van Roozendaal and reviewed by three anonymous referees.

¹²Joint Center for Earth Systems Technology, University of Maryland Baltimore County, Baltimore, MD 21250, USA

Abstract

NASA's Deriving Information on Surface Conditions from Column and Vertically Resolved Observations Relevant to Air Quality (DISCOVER-AQ, conducted in 2011–2014) campaign in the United States and the joint NASA and National Institute of Environmental Research (NIER) Korea–United States Air Quality Study (KORUS-AQ, conducted in 2016) in South Korea were two field study programs that provided comprehensive, integrated datasets of airborne and surface observations of atmospheric constituents, including nitrogen dioxide (NO₂), with the goal of improving the interpretation of spaceborne remote sensing data. Various types of NO₂ measurements were made, including in situ concentrations and column amounts of NO₂ using ground- and aircraft-based instruments, while NO₂ column amounts were being derived from the Ozone Monitoring Instrument (OMI) on the Aura satellite. This study takes advantage of these unique datasets by first evaluating in situ data taken from two different instruments on the same aircraft platform, comparing coincidentally sampled profile-integrated columns from aircraft spirals with remotely sensed column observations from ground-based Pandora spectrometers, intercomparing column observations from the ground (Pandora), aircraft (in situ vertical spirals), and space (OMI), and evaluating NO₂ simulations from coarse Global Modeling Initiative (GMI) and high-resolution regional models. We then use these data to interpret observed discrepancies due to differences in sampling and deficiencies in the data reduction process. Finally, we assess satellite retrieval sensitivity to observed and modeled a priori NO₂ profiles. Contemporaneous measurements from two aircraft instruments that likely sample similar air masses generally agree very well but are also found to differ in integrated columns by up to 31.9 %. These show even larger differences with Pandora, reaching up to 53.9 %, potentially due to a combination of strong gradients in NO₂ fields that could be missed by aircraft spirals and errors in the Pandora retrievals. OMI NO₂ values are about a factor of 2 lower in these highly polluted environments due in part to inaccurate retrieval assumptions (e.g., a priori profiles) but mostly to OMI's large footprint (> 312 km²).

1 Introduction

Nitrogen dioxide (NO₂) plays an important role in the troposphere by altering ozone production and OH radical concentration (Murray et al., 2012, 2014). It is one of the six United States Environmental Protection Agency (EPA) criteria pollutants because of its adverse health effects on humans (WHO, 2013). Major sources of nitrogen oxides (NO_x=NO + NO₂) in the troposphere include combustion, soil, and lightning. As a trace gas with a relatively short lifetime, NO₂ is usually confined to a local scale with respect to its source and therefore exhibits strong spatial and temporal variations, leading to difficulties in comparing NO₂ observations by methods with different atmospheric sampling.

Due to its distinct absorption features at ultraviolet–visible (UV–Vis) wavelengths, atmospheric NO₂ is observable from ground- and space-based remote sensing instruments. In particular, space-based measurements of tropospheric column NO₂ have been widely used to study spatial and temporal patterns (e.g., Beirle et al., 2003; Richter et al., 2005; Boersma

et al., 2008; Lu and Streets, 2012; Wang et al., 2012; Hilboll et al., 2013; Russell et al., 2010, 2012; Duncan et al., 2013; Lin et al., 2015) as well as long-term trends (e.g., van der A et al., 2008; Lamsal et al., 2015; Krotkov et al., 2016), and to infer NO_x sources (e.g., Jaeglé et al., 2005; van der A et al., 2008; Bucsela et al., 2010; de Wildt et al., 2012; Lin, 2012; Ghude et al., 2010; Ghude et al., 2013a; Mebust and Cohen, 2013; Pickering et al., 2016) and top-down NO_x emissions (e.g., Martin et al., 2003; Konovalov et al., 2006; Zhao and Wang, 2009; Lin et al., 2010; Lamsal et al., 2011; Ghude et al., 2013b; Vinken et al., 2014; Schreier et al., 2015; Cooper et al., 2017; Miyazaki et al., 2017; Liu et al., 2018). These observations have also been often used to assess chemical mechanisms (e.g., Martin et al., 2002; van Noije et al., 2006; Lamsal et al., 2008; Kim et al., 2009; Herron-Thorpe et al., 2010; Huijnen et al., 2010) and to infer the lifetime of NO_x (e.g., Schaub et al., 2007; Lamsal et al., 2010; Beirle et al., 2011) in chemical transport models (CTMs). Surface NO_2 concentrations (Lamsal et al., 2008, 2014; Novotny et al., 2011; Bechle et al., 2013) and NO_x deposition flux (Nowlan et al., 2014; Geddes and Martin, 2017) can also be estimated using satellite NO_2 observations. As the accuracy of any application of satellite data largely depends on the data quality, validation of satellite NO_2 observations is necessary.

A number of validation studies of space-based tropospheric NO_2 columns have been conducted using independent NO_2 observations from airborne in situ mixing ratio measurements (e.g., Boersma et al., 2008; Bucsela et al., 2008; Hains et al., 2010; Lamsal et al., 2014), ground-based total column (e.g., Pandora instrument; Herman et al., 2009) and tropospheric (MAX-DOAS instrument; e.g., Vlemmix et al., 2010; Irie et al., 2012) column measurements, and airborne high-resolution differential optical absorption spectroscopy (DOAS) measurements (Lamsal et al., 2017; Nowlan et al., 2018). Most validation studies utilizing in situ and ground-based observations have reported that satellite measurements tend to underestimate tropospheric NO_2 columns, especially over highly polluted areas (e.g., Hains et al., 2010). Intrinsic limits of space-based measurements, however, pose a challenge in comparisons between satellite, in situ, and ground-based measurements due to differences in representativeness. As stated above, NO_2 usually exhibits very sharp spatial gradients (tens of meters to kilometers). In contrast, the spatial resolution of satellite measurements is too coarse (tens of kilometers) to capture the fine spatial features of tropospheric NO_2 abundance. Therefore, it is important to recognize and account for the spatial variability while comparing satellite data with ground-based and in situ observations.

While the intrinsic resolution of satellite observations cannot be altered, there are ways to improve the derived satellite data products. The fidelity of the retrieved NO_2 product is dependent on the assumptions (e.g., NO_2 vertical profile shape, surface reflectivity) made in the retrieval algorithm. Some of the input parameters are available at much coarser resolution than the spatial resolution of OMI, introducing spatially (e.g., rural-to-urban) varying retrieval biases. Several studies show that the use of high-resolution NO_2 profiles results in significant improvements in retrievals (e.g., Russell et al., 2012; Lin et al., 2014; Lamsal et al., 2014; McLinden et al., 2014; Laughner et al., 2016, 2019; Goldberg et al., 2017). Deficiencies in model distributions of NO_2 may be identified and improved through rigorous evaluation with independent data, such as the suite of data collected during the Deriving Information on Surface Conditions from Column and Vertically Resolved Observations Relevant to Air Quality (DISCOVER-AQ) campaign deployments.

In this paper, we use comprehensive, integrated datasets of NO₂ gathered from surface, aircraft, and space instruments during NASA DISCOVER-AQ and the NASA and National Institute of Environmental Research (NIER) Korea–United States Air Quality Study (KORUS-AQ) together with NO₂ model simulations to address questions regarding retrieval accuracy. We describe the datasets in Sect. 2.1 and the models in Sect. 2.2. As an example, we focus on the NASA Standard NO₂ Product from OMI onboard the Aura satellite and conduct retrieval studies using the algorithm as discussed in Sect. 2.3, but the approaches discussed here could be applied to similar products as well. Results are presented in Sect. 3.

2 Observations and chemical transport models

2.1 NO₂ observations during DISCOVER-AQ and KORUS-AQ field campaigns

DISCOVER-AQ (<https://www-air.larc.nasa.gov/missions/discover-aq/>, last access: 5 September 2019) and KORUS-AQ (<https://www-air.larc.nasa.gov/missions/korus-aq/>, last access: 5 September 2019) were field study programs that provided comprehensive, integrated datasets of airborne and surface observations relevant to the diagnosis of surface air quality conditions from space. DISCOVER-AQ was a part of the NASA Earth Venture program and conducted four field deployments in Maryland (MD), California (CA), Texas (TX), and Colorado (CO) that covered different seasons and pollution regimes. KORUS-AQ was an international cooperation field study program conducted in the Republic of Korea (South Korea), sponsored by NASA and the South Korean government through the NIER. Table 1 summarizes the campaign locations and periods for the two field campaigns.

The primary objectives of DISCOVER-AQ and KORUS-AQ included (1) exploring the relationship between air quality at the surface and the tropospheric columns that can be derived from satellite orbit, (2) examining the diurnal variation of these relationships, and (3) characterizing the scales of variability relevant to the model simulation and remote observation of air quality. To accomplish these objectives, an observing strategy was designed to carry out systematic and concurrent in situ and remote sensing observations from a network of ground sites and research aircraft. The payloads on research aircraft consisted of several in situ instruments that differed minimally between campaigns. Ground-based trace gas observations included in situ surface and remote sensing Pandora measurements (Herman et al., 2009).

Figure 1 illustrates a conceptual view of the instruments and their sampling methods with their areal coverage for NO₂ observations. While the aircraft (P-3B for DISCOVER-AQ and DC-8 for KORUS-AQ) make spirals (P-3B) or ascents and descents (DC-8) over the site, the onboard National Center for Atmospheric Research (NCAR) and thermal dissociation laser-induced fluorescence (TD-LIF) instruments measure in situ NO₂ profiles. The aircraft usually visit each site two to four times a day to observe the diurnal variations of the NO₂ profiles. The P-3B aircraft made spirals of ~ 4 km diameter, whereas the DC-8 ascents and descents covered 10–20 km. Consequently, the distance between the ground and aircraft locations was 0–5 km during the DISCOVER-AQ and 10–20 km during the KORUS-AQ campaign. Pandora and NO₂ ground monitor instruments are typically located at ground stations close to the aircraft profiles. Throughout the day, Pandora reports the total column NO₂ from direct-sun measurements, and the ground monitor reports the in situ surface NO₂ mixing

ratio. Finally, OMI retrievals report a tropospheric column NO₂ once a day in the afternoon; the OMI pixel has a much larger ground footprint compared with the in situ and Pandora measurements. Table 2 lists the sites with ground-based NO₂ monitors used in this analysis, along with the type of instrument employed at each site and the numbers of aircraft profiles and Pandora measurements available from each site near the time of OMI overpass. Detailed data descriptions follow in this section.

2.1.1 Vertical distribution of NO₂ by aircraft—In situ NO₂ volume mixing ratios (VMRs) were measured from the NASA P-3B (DISCOVER-AQ) and DC-8 (KORUS-AQ) aircraft. The number of flights varied between campaigns, ranging from 10 for Texas to 22 for Korea. Flights took place during a range of conditions, e.g., pollution episodes, clean days, weekdays, and weekends. Measurements usually commenced in the morning and continued throughout the day with multiple sorties on a given day. During each sortie, the aircraft made vertical spirals over surface sites, sampling NO₂ between ~ 300 m and 5 km from the Earth's surface. In Maryland, spirals were also made over the Chesapeake Bay area, which did not have any ground monitors.

Airborne measurements were carried out using two different instruments and measurement techniques. The four-channel chemiluminescence instrument from the National Center for Atmospheric Research (NCAR) measured NO₂ by the photolysis of NO₂ and subsequent chemiluminescence detection of NO₂ following the oxidation of the photolysis product NO with ozone (Ridley and Grahek, 1990). This instrument has an NO₂ measurement uncertainty of 10 % and a 1 s, 2 σ detection limit of 50 parts per trillion by volume (pptv). We hereafter refer to these NO₂ measurements as “NCAR”. The thermal dissociation laser-induced fluorescence (TD-LIF) method used by the University of Berkeley detects NO₂ directly and other nitrogen species (e.g., total peroxy nitrates, alkyl nitrates, HNO₃) following the thermal dissociation of all oxides of nitrogen (NO_x) to NO₂ (Thornton et al., 2000). The laser-induced fluorescence method is highly sensitive for measuring NO₂, with a detection limit of 30 pptv. The measurement uncertainty is 5 %. This instrument has a lower NO₂ sampling frequency than the NCAR instrument due to its alternating measurement cycle for different species. We refer to these NO₂ measurements as TD-LIF.

Here we use 1 s merged data provided in the campaign data archives and focus on early afternoon measurements made within 1.5 h of the OMI overpass time (13:45 approximately). This time window of ± 1.5 h is selected to maximize the number of samples while reducing effects from the diurnal variation of NO₂. Figure 2 shows the mean NO₂ profile for each of the DISCOVER-AQ and KORUS-AQ campaigns. Measurements show considerable spatiotemporal variation as well as some indication of a well-developed mixing layer, with the maximum mixing ratio near the ground. The mixing layer heights vary by region and season. For example, in the MD campaign conducted in summer, the mixing layer stretches up to 800 hPa (2 km). In contrast, the mean profiles from the CA campaign conducted in winter show a shallow mixing layer extending only up to 950 hPa (~ 700 m). Near-surface NO₂ mixing ratios also vary by campaign location and possibly by season, with the highest near-surface NO₂ in CA. In South Korea, the mean near-surface NO₂ mixing ratio is not as high as in CA, but a very high (~ 5 ppbv) NO₂ mixing ratio stretches up to 850 hPa, resulting in the greatest NO₂ column. While the NCAR and TD-LIF mean

profiles generally agree with each other in the MD, CA, and CO campaigns, they exhibit larger differences in TX and South Korea. Figure 2 also shows the nature of the variability in observed and simulated NO₂ vertical profiles over the campaign domains. The observed differences between the model and observations arise primarily from a mismatch in both spatial and temporal sampling. The use of more restrictive collocation (spatial and temporal) applied for comparing different datasets in Sect. 3.1 and examining the air mass factor (AMF) effect in Sect. 2.3.2 would have resulted in different vertical distributions.

2.1.2 In situ surface NO₂ measurements—To extend the altitude range of the vertical profiles discussed in Sect. 2.1.1, we merge in situ aircraft profile measurements with coincident in situ surface NO₂ measurements sampled over the duration of spirals (~ 20 min) by linearly interpolating the NO₂ mixing ratios between the surface and the lowest aircraft altitudes. These new merged profiles contain a greater portion of the tropospheric NO₂ column. During both the DISCOVER-AQ and KORUS-AQ campaigns, in situ surface NO₂ monitors were deployed at several ground sites (Table 2). Measurements were carried out using one of four different types of NO₂ monitors, including a chemiluminescence NO_x monitor equipped with either a molybdenum or photolytic converter, a cavity-attenuated phase shift (CAPS) spectrometer, and a cavity ring-down spectrometer (CRDS). The molybdenum converter analyzer measures NO₂ indirectly by the thermal conversion of NO₂ to NO using molybdenum and the detection of NO by chemiluminescence that results from the reaction of NO with ozone. Since the reduction process could convert not only NO₂ but also other reactive nitrogen species, this instrument could overestimate NO₂ concentrations (Dunlea et al., 2007; Steinbacher et al., 2007; Lamsal et al., 2008; Dickerson et al., 2019). The magnitude of interference depends on the relative concentrations of NO₂, nitric acid, alkyl nitrates, and peroxy-acetyl nitrate, which vary spatially, diurnally, and seasonally and are difficult to quantify. Considering their use in the sections below (Sects. 2.3.2 and 3), we conducted a sensitivity study examining how 0 %–50 % biases in molybdenum converter measurements could impact tropospheric columns derived from merged (aircraft + surface) profiles. We found that the errors are usually rather small at < 6 % for various sites. Therefore, no attempt is made here to correct for the interference in these measurements, although we identify those sites in Table 2 and Fig. 6.

The operating principle of a photolytic converter analyzer is also gas-phase chemiluminescence, but the use of a photolytic converter to reduce NO₂ to NO makes it more specific to NO₂. As a result, this instrument provides nearly interference-free NO₂ measurements, with the exception of nitrous acid (HONO; Ryerson et al., 2000). Measurement uncertainties for 1 h averages are expected to be ~ 10 % (Fehsenfeld et al., 1990).

The CAPS instrument detects NO₂ by measuring absorption around 450 nm. Baseline measurements spanning minutes to hours with a source of NO₂-free air are needed to determine NO₂ amounts. In contrast to the chemiluminescence–molybdenum converter techniques, CAPS directly detects NO₂. Its specificity for NO₂ is affected by potential interference from species like glyoxal, water vapor, and ozone that absorb light within the band pass of the instrument. The detection limit is < 0.1 ppb for a 10 s measurement. NO₂

measurements from CAPS and chemiluminescence NO_x monitors with a molybdenum converter are reported to agree to within 2 % (Kebabian et al., 2008).

A CRDS is a sensitive and compact detector that measures multiple nitrogen species including NO_2 . It employs a laser diode at 405 nm for the direct detection of NO_2 . Interferences arising from absorption by other trace gases, such as ozone and water vapor, are expected to be small. The measurement precision is 20 ppt at a 1 s time resolution and the accuracy is better than 5 %, which is primarily limited by the NO_2 absorption cross section used in the data reduction process. The total reactive nitrogen (NO_y) measured by the CRDS and chemiluminescence NO_x monitor with a molybdenum converter is found to agree to within 12 % (Wild et al., 2014).

2.1.3 Pandora total column NO_2 —In addition to in situ measurements, each campaign hosted ground-based networks of Pandora instruments. Pandora is a small, commercially available sun-viewing spectrometer optimized for the detection of trace gases, including NO_2 . It measures direct solar spectra in the 280–525 nm spectral range with 0.6 nm resolution. A detailed description of the instrument’s design, operation, and retrieval method can be found in Herman et al. (2009, 2018). The NO_2 retrieval algorithm includes (1) a direct-sun spectral fitting method similar to traditional differential optical absorption spectroscopy (DOAS) (Platt, 1994) using one measurement (or an average of several measurements) as a reference spectrum to derive relative NO_2 slant column densities (SCDs), (2) the application of the Modified Langley Extrapolation (MLE) to derive total NO_2 SCDs, and (3) the conversion of total NO_2 SCDs to vertical column densities (VCDs) using the direct-sun air mass factor (AMF) as follows:

$$\text{VCD} = \text{SCD}/\text{AMF} . \quad (1)$$

The spectral fitting is performed over the 400–440 nm window; it fits NO_2 cross sections at 254.5 K (Vandaele et al., 1998), ozone (Brion et al., 1993), and a fourth-order smoothing polynomial, and it applies a wavelength shift and a constant offset. In clear-sky conditions, this instrument provides total NO_2 VCD with a precision of 2.7×10^{14} and an absolute accuracy of 1.3×10^{15} molec cm^{-2} (Herman et al., 2018). Potential sources of error in NO_2 retrievals include the calibration of raw data, the chosen reference spectrum, and the use of a fixed temperature for the NO_2 cross section. Pandora NO_2 data have been compared with data from direct-sun multifunction DOAS (MFDOAS) and Fourier transform ultraviolet spectrometry (UVFTS) (Herman et al., 2009) and have been found to agree within 12 %. These data are regularly used to validate satellite NO_2 retrievals (e.g., Lamsal et al., 2014; Tzortziou et al., 2015, 2018; Ialongo et al., 2016).

Here, we use clear-sky quality-controlled (root mean square (rms) < 0.05 and errors < 0.05 DU) 80 s total column NO_2 data averaged over the duration of each aircraft spiral. We infer tropospheric column NO_2 by subtracting the OMI stratospheric column from the Pandora total column to compare with tropospheric NO_2 from in situ and OMI observations.

2.2 NO₂ simulations

2.2.1 GMI simulation—The Global Modeling Initiative (GMI) three-dimensional chemical transport model (CTM) simulates the troposphere and stratosphere (Strahan et al., 2013) with a stratosphere–troposphere chemical mechanism (Duncan et al., 2007) updated with the latest chemical rate coefficients (Burkholder et al., 2015) and time-dependent natural and anthropogenic emissions (Strode et al., 2015). Aerosol fields are computed online with the Goddard Chemistry Aerosol Radiation and Transport (GOCART) model (Chin et al., 2014, and references therein). Tropospheric processes such as NO_x production by lightning, scavenging, and wet and dry deposition are also represented in the model. The GMI simulations used in this work were constrained with meteorology from the Modern-Era Retrospective Analysis for Research and Applications version 2 (MERRA-2) meteorological fields (Gelaro et al., 2017) at 72 vertical levels from the surface to 0.01 hPa, with a resolution ranging from 150 m in the boundary layer to ~ 1 km in the upper troposphere and lower stratosphere, and at a horizontal spatial resolution of 1.25° longitude × 1.0° latitude.

GMI simulations have been evaluated in the troposphere and stratosphere. Strode et al. (2015) showed good agreement with tropospheric O₃ and NO_x trends in the US in a 1990–2013 hindcast simulation. Strahan et al. (2016) demonstrated realistic seasonal and interannual variability of Arctic composition using comparisons to Aura MLS O₃ and N₂O. The simulation of NO₂ in both the troposphere (Lamsal et al., 2014) and stratosphere (Spinei et al., 2014; Marchenko et al., 2015) has been shown to be in good agreement with independent measurements. We sample the model profile at the times and locations of airborne measurements. Figure 2 compares GMI NO₂ profiles with collocated aircraft measurements during the DISCOVER-AQ and KORUS-AQ field campaigns. The GMI simulation generally captures the vertical distribution of NO₂ in the free troposphere, is somewhat lower in the middle and upper parts of the mixing layer, and exhibits sharper gradients between the boundary layer and the surface. Due to the coarse spatial resolution of the GMI model, the surface pressure of the GMI profiles differs from the measurements, especially over complex terrain in CA, CO, and Korea.

2.2.2 NO₂ simulations using regional models—For each DISCOVER-AQ and KORUS-AQ deployment, a high-resolution model simulation was conducted. We use NO₂ profiles from those simulations to examine their effect on retrievals in Sect. 2.3.2 and to downscale OMI NO₂ retrievals in Sect. 2.3.3. Below we provide a brief description of each simulation. Information about model options for these simulations can be found in Table A1 in the Appendix. For most of the campaigns, the near-surface NO₂ concentration and the model profile shapes agree in general with the NCAR and TD-LIF profiles. In TX, however, the CMAQ simulation shows lower mixing ratios than observations throughout the mixing layer (Fig. 2).

MD. The Weather Research and Forecasting (WRF) model was run (Loughner et al., 2014) from 24 May through 1 August 2011 at horizontal resolutions of 36, 12, 4, and 1.33 km with 45 vertical levels from the surface to 100 hPa with 16 levels within the lowest 2 km. Meteorological initial and boundary conditions were taken from the 12 km North American Mesoscale (NAM) model. Output from the 4 and 1.33 km WRF simulations were fed into

the Community Multiscale Air Quality (CMAQ; Byun and Schere, 2005). Chemical initial and boundary conditions for the 4 km CMAQ run came from a 12 km CMAQ simulation covering the continental US, which was performed for the GEO-CAPE Regional Observing System Simulation Experiment (OSSE). The creation of the emissions used within the CMAQ simulation is described in Loughner et al. (2014) and Anderson et al. (2014). CMAQ was run with reduced mobile emissions by 50 % and an increase in the photolysis frequency of organic nitrate species based on Anderson et al. (2014).

CA. The coupled WRF–CMAQ modeling system (Wong et al., 2012) was run from 1 January through 28 February 2013 (2013 DISCOVER-AQ California campaign period) at horizontal resolutions of 4 and 2 km, with 35 vertical levels from the surface to 50 hPa and an average height of the middle of the lowest layer of 20 m. WRF version 3.8 and CMAQ version 5.2.1 were used in a coupled format, allowing for frequent communication between the meteorological and chemical transport models and indirect effects from aerosol loading on the meteorological calculations in WRF. Meteorological initial and boundary conditions were taken from the 12 km NAM reanalysis product from NOAA statistical and mathematical symbols. Observation nudging above the planetary boundary layer (PBL) using four-dimensional data assimilation (FDDA) was applied in WRF. Chemical initial and boundary conditions for the 4 km CMAQ simulation came from a 12 km CMAQ simulation covering the continental US, while initial and boundary conditions for the 2 km simulation were obtained from the 4 km WRF–CMAQ simulation. Emissions are based on the 2011 US National Emissions Inventory (NEI) with year-specific updates to point and mobile sources, while biogenic emissions were calculated inline in CMAQ using the Biogenic Emissions Inventory System (BEIS).

TX. To simulate the DISCOVER-AQ Texas campaign, a WRF model simulation was performed from 18 August through 1 October 2013, covering the entire field deployment in September 2013. The model was run at 36, 12, 4, and 1.33 km horizontal resolutions with 45 levels from the surface to 50 hPa. Meteorological initial and boundary conditions were taken from the 12 km North American Mesoscale (NAM) model. Output from the 4 and 1.33 km simulations were used to run the CMAQ model. Chemical and initial boundary conditions for the outer domain were taken from the Model for Ozone and Related chemical Tracers (MOZART) chemical transport model (CTM). Detailed information about these simulations and the emissions used can be found at http://aqrp.ceer.utexas.edu/projectinfoFY14_15/14-004/14-004FinalReport.pdf (last access: 5 September 2019).

CO. For the Colorado deployment, WRF was run from 9 July through 20 August 2014 at spatial resolutions of 12 km (covering the western US) and 4 km (covering Colorado). The model top was set at 50 hPa, with 37 levels in the vertical. Analysis fields from the European Centre for Medium-Range Weather Forecasts (ECMWF) were used for meteorological initial and boundary conditions. Chemical initial and boundary conditions for the outer domain were taken from Real Time Air Quality Monitoring System (RAQMS) model output. Further information about this simulation can be found at https://www.colorado.gov/airquality/tech_doc_repository.aspx?action=open&file=FRAPPE-NCAR_Final_Report_July2017.pdf (last access: 5 September 2019).

Korea. Air quality forecasts were performed using the Weather Research and Forecasting model (Skamarock et al., 2008) coupled to the Chemistry (WRF-Chem) (Grell et al., 2005) model to support KORUS-AQ flight planning and post-campaign analysis. The modeling domains consist of a regional domain of 20 km resolution covering major sources of transboundary pollutants affecting the Korean Peninsula: anthropogenic pollution from eastern China, dust from inner China and Mongolia, and wildfires from Siberia (Saide et al., 2014). A 4 km resolution domain was nested and covered the Korean Peninsula and surroundings, which encompassed the region where the DC-8 flights were planned and better resolved local sources. Anthropogenic emissions were developed by Konkuk University for KORUS-AQ forecasting and are described in Goldberg et al. (2019).

2.3 OMI NO₂ observations

The Ozone Monitoring Instrument (OMI) aboard the NASA Aura satellite provides measurements of solar backscatter that are used to retrieve total, stratospheric, and tropospheric NO₂ columns with a native ground resolution varying from 13km × 24km near nadir to 40km × 250km at swath edges (Levelt et al., 2006, 2018). The Aura satellite was launched on 15 July 2004 into a sun-synchronous polar orbit with a local Equator crossing time of 13:45 in the ascending node. OMI is one of the most stable UV–Vis satellite instruments providing a long-term high-resolution data record with low degradation (Dobber et al., 2008; DeLand and Marchenko, 2013; Schenkeveld et al., 2017). In the middle of 2007, an anomaly began to appear in OMI radiances in certain rows affecting all Level 2 products (Schenkeveld et al., 2017). This “row anomaly” can be easily identified, and the affected rows are discarded. We use OMI pixels with a cloud radiance fraction less than 50 % and quality flags indicating good data.

2.3.1 Standard OMI NO₂ Product—Here we use the Standard OMI NO₂ Product (OMNO₂) version 3.1, with updates from version 3.0 (Krotkov et al., 2017). The NO₂ retrieval algorithm uses the differential optical absorption spectroscopy (DOAS) technique. The retrieval method includes (1) the determination of NO₂ slant column density (SCD) using a DOAS spectral fit of the NO₂ cross section from measured reflectance spectra over the 402–465 nm range; (2) the calculation of an air mass factor (AMF) that is required to convert SCD into vertical column density (VCD); and (3) a scheme to separate stratospheric and tropospheric VCDs. The AMF calculation is performed by combining NO₂ measurement sensitivity (scattering weights) from the TOMS RADiative transfer model (TOMRAD; Dave, 1964) with the a priori relative vertical distribution (profile shape) of NO₂ taken from the GMI CTM. Computation of scattering weights requires information on viewing and solar geometries, terrain and cloud reflectivities, terrain and cloud pressures, and cloud cover (radiative cloud fraction).

The version used here represents a significant advance over previous versions (Bucsela et al., 2006, 2013; Celarier et al., 2008; Lamsal et al., 2014). It includes an improved DOAS algorithm for retrieving slant column densities (SCDs) as discussed in Marchenko et al. (2015). The key features of the algorithm include more accurate wavelength registration between Earth radiance and solar irradiance spectra, iterative accounting of the rotational Raman scattering effect, and sequential SCD retrieval of NO₂ and interfering species (water

vapor and glyoxal). Solar irradiance reference spectra are monthly average data derived from OMI measurements instead of an OMI composite solar spectrum used in prior versions. Cloud pressure and cloud fraction are taken from an updated version of the OMCLDO2 cloud product that includes updated lookup tables and O₂–O₂ SCD retrieved with a temperature correction (Veefkind et al., 2016). A priori NO₂ profiles are as discussed in Lamsal et al. (2015) and Krotkov et al. (2017) and use 1° latitude 1.25° longitude GMI model-based monthly a priori NO₂ profiles with year-specific emissions. This retrieval version also uses more accurate information on terrain pressure that is calculated from high-resolution digital elevation model (DEM) data at 3 km resolution and GMI terrain pressure.

2.3.2 Recalculation of OMI NO₂ AMF using alternative NO₂ profiles—NO₂

vertical profiles, especially in the troposphere, vary strongly in both space and time. The simulated NO₂ profiles from a global CTM (GMI) employed in the operational NO₂ retrieval, while offering a good option at a global scale, may not sufficiently capture the distribution of NO₂ at OMI's ground resolution. Using precalculated scattering weights (*Sw*) made available in the OMNO2 product and alternative information on vertical NO₂ profile shape (*X_a*), the OMI NO₂ AMF can be readily recalculated (Lamsal et al., 2014):

$$\text{AMF}_{\text{trop}} = \frac{\sum_{\text{surface}}^{\text{tropopause}} \text{Sw} \cdot X_a}{\sum_{\text{surface}}^{\text{tropopause}} X_a}, \quad (2)$$

where the integral from the surface to the tropopause yields the tropospheric AMF (AMF_{trop}). Scattering weights vary with viewing and solar geometry, cloud–aerosol conditions, and surface reflectivity, but they are assumed to be independent of the vertical distribution of NO₂. The typical vertical distribution of scattering weights is characterized by lower values in the troposphere due to reduced sensitivity owing to Rayleigh scattering and higher values (corresponding to a nearly geometric AMF) in the stratosphere. The AMF is therefore highly sensitive to NO₂ profile shape in the lower troposphere.

Here, we investigate how a priori NO₂ profiles affect OMI tropospheric AMF and consequently the retrieval of OMI tropospheric NO₂ VCD. For this, we combine the measured profile (from the surface to ~ 5 km) with coincidentally sampled simulated NO₂ from GMI (5 km to the tropopause) to create a complete tropospheric NO₂ profile. We choose the GMI simulation over the high-resolution model simulations because we found that the GMI generally better performed in the free troposphere compared to the regional models. We then interpolate the pressure-tagged NO₂ observations (aircraft NCAR NO₂ + surface) onto the pressure grid of the OMI NO₂ scattering weight. The tropospheric AMFs obtained using individual measured profiles (AMF_{obs}) are compared with the AMFs in the OMI Standard Product (AMF_{SP}), which are calculated using the GMI yearly varying monthly climatology (Fig. 3a). AMF_{SP} is generally higher than AMF_{obs} by 34 % on average, with the largest difference (61.6 %) for TX and the smallest difference (16.6 %) for Korea; this means that the OMI SP VCDs, based on the AMF_{SP} , are correspondingly smaller on average than the those based on measured profiles. The correlation ranges from fair ($r = 0.41$, $N = 21$) for MD and TX to excellent ($r = 0.92$, $N = 36$) for CA and Korea, with the overall correlation coefficient of 0.53.

To explore how NO₂ profiles from high-resolution model simulations could affect OMI NO₂ retrievals, we calculate tropospheric AMFs using simulated monthly NO₂ profiles (AMF_{HR}). Since the OMI ground pixel size is much larger than the model grid boxes, we derive an average profile of all model grid boxes located within one OMI pixel and use it to calculate AMF_{HR}. Figure 3b compares AMF_{obs} with AMF_{HR}; it suggests improved agreement compared to AMF_{SP} (Fig. 3a), especially for CA, CO, and Korea, although with no significant improvement in the correlation.

We also considered how using AMFs based on monthly mean profiles, such as the OMI SP, impacts retrieved NO₂. To assess this, we calculated AMFs using both daily (AMF_{obs}) and campaign-average measured NO₂ profiles (AMF_{obs-m}). Figure 3c shows that AMF_{obs} and AMF_{obs-m} agree to within 5.3 % and exhibit excellent correlation ($r > 0.8$). That is, the use of a mean profile does not make a significant difference compared to the individual daily profiles, implying that the average profile generally captures the local vertical distribution fairly well. Somewhat larger scatter in TX may be related to stronger land–sea breeze dynamics that could affect the vertical distribution of NO₂ in both the boundary layer and free troposphere. Our results here differ from previous studies that reported improved agreement of OMI NO₂ retrievals using simulated daily NO₂ profiles with independent observations (Valin et al., 2013; Laughner et al., 2019), although Laughner et al. (2019) also suggested poorer performance with daily profiles in the southeast US than in other regions.

2.3.3 Downscaled OMI NO₂ data—The NO₂ value associated with an OMI ground pixel is averaged over a large area. This spatial smoothing leads to a loss of information on sub-pixel variation, which could be considerable for NO₂, especially over urban source regions. Therefore, it is important to recognize and address this limitation while assessing, interpreting, and using satellite NO₂ data. Here we use high-resolution NO₂ model simulations for sub-pixel variation.

We apply the method described by Kim et al. (2016, 2018) to downscale OMI NO₂ retrievals, which are then compared with aircraft and Pandora data. This method applies high-resolution model-derived spatial-weighting kernels to individual OMI pixels and calculates sub-pixel variability within the pixel. The major assumption is that the model captures the spatial distribution of emission sources and NO₂ transport patterns well. The method ensures that the quantity (total number of molecules) of the satellite data over the pixel is numerically preserved, while adding higher-resolution spatial information to the derived tropospheric NO₂ columns.

Figure 4 illustrates the downscaling of tropospheric NO₂ for an OMI pixel using the high-resolution CMAQ simulation over Essex, Maryland. The tropospheric NO₂ column observed by OMI (5.9×10^{15} molec cm⁻²) is 25.7 % higher than the average of the CMAQ NO₂ columns over the pixel. The spatial-weighting kernels suggest more than an order of magnitude difference in NO₂ within this single OMI pixel. Applying the kernels to the original OMI pixel value results in a range of sub-pixel NO₂ column values from 1.9×10^{15} over a clean background to 3.2×10^{16} molec cm⁻² over a polluted hot spot.

Figure 5 demonstrates how the downscaled OMI NO₂ data using high-resolution NO₂ output from a CMAQ simulation compare with the original OMI NO₂ data from the standard product. Both OMI SP and CMAQ show enhanced NO₂ columns at major urban areas, but their magnitudes differ, with OMI showing lower values. As described above, OMI's field of view covers a large area, sampling the NO₂ field over the entire pixel, while the actual NO₂ distribution (better resolved by the CMAQ simulation) is defined by local source strengths, chemistry, and wind patterns that can occur at much finer spatial scales. By employing the relative ratios inside an OMI pixel rather than the overall magnitude of simulated columns, the downscaling technique yields a more detailed structure, enhancing NO₂ over sources and dampening it elsewhere by more than a factor of 2.

3 Results and discussion

3.1 Comparison between in situ observations

Figure 6a and Table 3 summarize how the two airborne in situ NO₂ tropospheric column measurements compare. We derive the column amount by first extending the NCAR and TD-LIF NO₂ profiles to the same surface NO₂ concentration measurements and then integrating the NO₂ profiles. The only exception is at the Chesapeake Bay during the MD campaign, the only marine site used in this study; we extend a constant NO₂ mixing ratio measured at the lowest aircraft altitudes to the surface. To compare with OMI and Pandora retrievals, NO₂ amounts for the missing portion from the top of the aircraft altitude to the tropopause are added from the GMI simulation. This amount varied between 4.7×10^{14} and 1.2×10^{15} molec cm⁻² and represented an average 5 % of the tropospheric NO₂ columns but can reach up to 50.8 % for an individual profile. Overall, the two airborne in situ columns generally agree very well and exhibit excellent correlation ($r = 0.87\text{--}0.99$). The correlation and mean difference differ among the five campaigns, with TD-LIF higher than NCAR by 31.9 % in TX and 11.6 % in Korea but lower by ~ 10% in MD and CO. The observed difference in TX is much larger than the reported uncertainty of both NCAR and TD-LIF measurements. Analysis of individual profiles suggests that the data from TD-LIF are generally higher than NCAR at all altitudes, regardless of the NO₂ pollution level (Fig. 7). The underlying cause of this difference is not clear, but it may be associated with the applied calibration standard or an interference issue for either or both of the two measurements. The small difference elsewhere could come from the lower measurement frequency of TD-LIF compared with the NCAR instrument.

3.2 Comparison between Pandora and aircraft observations

Figure 6b–c and Table 3 show the comparison between Pandora and the two airborne tropospheric NO₂ column measurements. We derive tropospheric columns from Pandora by subtracting collocated OMI stratospheric NO₂ columns from the Pandora total column NO₂ retrievals. The relationship between the aircraft and Pandora data is not as good as between the two aircraft measurements themselves. The use of OMI stratospheric NO₂ columns to derive tropospheric columns from Pandora could impact the comparison between Pandora and aircraft observations; this approach is unlikely to be a significant factor over the polluted DISCOVER-AQ and KORUS-AQ campaign domains. The correlation ranges from fair ($r = 0.42$) to excellent ($r = 0.95$) for NCAR versus Pandora and poor ($r = 0.18$) to excellent ($r =$

0.94) for TD-LIF versus Pandora. The overall correlation coefficients between Pandora and the airborne NCAR and TD-LIF measurements are 0.94 and 0.91, respectively, with higher correlation in CO, TX, and Korea and lower correlation in MD and CA. Pandora data are about a factor of 2 lower than aircraft measurements in TX. Elsewhere, Pandora data agree with aircraft measurements to within 20 % on average, although much larger differences are observed for individual sites. A larger discrepancy for Pandora data in TX is also reported by Nowlan et al. (2018), who used various NO₂ measurements to evaluate GeoTASO NO₂ retrievals. The reasons for such exceptionally large differences could include strong gradients in the NO₂ field that are missed by aircraft spirals, errors in Pandora retrievals, or both.

3.3 Assessment of OMI NO₂ retrievals

We compare OMI tropospheric NO₂ columns with Pandora data and vertically integrated columns from aircraft spirals at 23 locations (Table 2) during the DISCOVER-AQ and KORUS-AQ field campaigns. We only analyze OMI pixels that overlap individual aircraft profiles. Spatially collocated aircraft and Pandora data are temporally matched to OMI by allowing only the measurements made within 1.5 h of the OMI overpass time. We infer tropospheric columns from Pandora by subtracting OMI-derived stratospheric NO₂ from Pandora total columns.

Figure 8a and b and Table A2 present tropospheric NO₂ columns from the OMI Standard Product compared with integrated columns from the NCAR and TD-LIF instruments. Although the OMI and aircraft data are significantly correlated ($r = 0.39\text{--}0.87$), OMI NO₂ retrievals are generally lower, with the largest difference in CO and the smallest difference in MD. OMI data are also lower than Pandora as shown in Fig. 8c. The magnitude of the difference and the degree of correlation with OMI vary for NCAR, TD-LIF, and Pandora measurements. This discrepancy between OMI, aircraft spiral columns, and Pandora local measurements is due to a combination of strong NO₂ spatial variation, the size of OMI pixels, and the placement of the sites, but OMI retrieval errors arising from inaccurate information in the AMF calculation, such as a priori NO₂ profiles, and potential errors in the validation sources themselves also contribute.

Figure 8d–f and Table A3 show the comparison after partially accounting for OMI retrieval errors arising from a priori NO₂ profiles taken from the GMI model. Replacing the model profiles with the NCAR and TD-LIF observed NO₂ profiles in the AMF calculations addresses the issues related to model inaccuracies, although the measured profiles may not necessarily represent the true average NO₂ over the entire OMI pixel (e.g., Fig. 4). Nevertheless, using observed profiles reduces OMI's mean differences with NCAR by 8 %–29.2 %, TD-LIF by 8.7 %–24.4 %, and Pandora by 6.8 %–24.2 %. Changes are largest in TX and smallest in CA and Korea. Correlations are either improved or remain similar.

Figure 8g–i and Table A4 show the comparison of OMI NO₂ columns derived using observed profiles with NCAR, TD-LIF, and Pandora observations after accounting for spatial variation in the NO₂ field as suggested by the CMAQ simulation. After downscaling, the agreement of OMI NO₂ columns improves further with NCAR by 1.1 %–41.5 %, TD-LIF by 1.2 %–39.7 %, and Pandora by 1.2 %–33.2 %. The exceptions are MD for both

aircraft and Pandora data and TX for Pandora data only. Changes are small in MD and Korea and large in CA and TX. The larger difference in TX is due to significant underestimation of NO₂ by Pandora instruments. The correlation improves in MD and TX but is reduced in CA, CO, and Korea. These results suggest that downscaling helps explain some of the discrepancies between OMI, aircraft, and Pandora observations. Variations among campaign locations may also point to difficulty related to the fidelity of the CMAQ simulations.

Figure 9 summarizes the comparison of OMI with aircraft and Pandora measurements. Here we present site mean columns observed from all measurements during the entire campaign periods. OMI captures the overall spatial variation in site means. In relatively cleaner places (NO₂ VCD $< 5 \times 10^{15}$ molec cm⁻²), OMI agrees well with NCAR and TD-LIF columns. OMI values are generally lower in polluted areas.

3.4 Implications for satellite NO₂ validations

NO₂ measurements from a variety of instruments and techniques taken during the DISCOVER-AQ and KORUS-AQ field deployments provided a unique opportunity to assess correlative data and realize the strengths and limitations of the various measurements. Some of the techniques are still in a state of development and evaluation, and the data have not been fully validated. Additional complications arise when comparing measurements covering different areal extents. This is particularly true for a short-lived trace gas like NO₂ that has a large spatial gradient, especially in the boundary layer.

The NCAR and TD-LIF instruments onboard the same aircraft (P-3B during DISCOVER-AQ and DC-8 during KORUS-AQ) offer valuable insights on the vertical distribution of NO₂, a critical piece of information needed for satellite retrievals. Despite their adjacent locations on the aircraft, they did not sample the same air mass throughout each profile due to their different NO₂ measurement frequencies. Despite this, and even using independent measurement techniques with unique sources of uncertainties, NO₂ measurements from the two instruments exhibit excellent correlation and very good agreement in most cases. However, varying discrepancies between the two instruments among campaigns with campaign-average differences reaching up to 31.9 % are unlikely to be related solely to the sampling issues; they are rather related to issues pertaining to measurement methods. It is crucial to reconcile these differences and improve the accuracy of these measurements for the meaningful validation and improved error characterization of satellite NO₂ retrievals.

In situ aircraft spirals miss significant portions of the tropospheric NO₂ column, especially from the ground to the lowest level of the aircraft altitude, typically 200–300 m above ground level. In this analysis, we account for the missing portion above the aircraft profile by using coincidentally sampled simulated NO₂ profiles. For the portion below the aircraft profile we extrapolate to surface monitor data. The latter step can be a significant error source, given that it assumes spatial homogeneity over the spiral domain. Additional errors could come from the use of different types of monitors that were deployed during the DISCOVER-AQ and KORUS-AQ campaigns (see Sect. 2.1.2). In particular, NO₂ data from molybdenum converter analyzers are biased high by variable amounts that are difficult to quantify and correct (e.g., Lamsal et al., 2008). The use of more accurate NO₂ monitors,

such as photolytic converter analyzers, together with balloon-borne NO₂ sondes (Sluis et al., 2010) of similar accuracy would complement in situ aircraft profiles.

While total column NO₂ retrievals from the ground-based remote sensing Pandora instrument are useful to track temporal changes, their use for satellite validation or for comparing with aircraft spiral data can be onerous, particularly over locations with large NO₂ spatial gradients, such as cities. Pandora's field of view is so narrow that it serves as a point measurement. Additionally, Pandora data are subject to retrieval errors arising predominantly from the use of an incorrect reference spectrum as well as fixed temperature for the NO₂ cross section in the spectral fitting procedure. Failure to apply a reference spectrum derived using weeks of measurements from the same site often yields systematic biases in the retrieved NO₂ columns. Improved calibration and data processing are therefore needed to improve the Pandora data quality. Concurrent spatial NO₂ observations from other ground-based (e.g., multi-axis differential optical absorption spectroscopy – MAX-DOAS; Vlemmix et al., 2010) or airborne (e.g., Geostationary Trace gas and Aerosol Sensor Optimization – GeoTASO; Nowlan et al., 2016; Judd et al., 2019) platforms would facilitate intercomparison among measurements of different spatial scales.

The validation of NO₂ observations from any satellite instrument, including OMI, is complicated by a variety of factors, principally the ground area covered by the instrument's field of view. As discussed in Sect. 3.3, disagreement between partially (spatially and temporally) matched OMI NO₂ and validation measurements made near sources may be reasonably anticipated and ought to be expected. Therefore, it may be necessary to use a proper validation strategy, such as downscaling of satellite data using either observed or modeled NO₂ as presented in Fig. 8g–i and Table A4. It also underscores the need for comprehensive high-quality long-term observations for validation. Enhanced agreement with OMI retrievals revised using observed NO₂ profiles is indicative of retrieval errors from model-based a priori vertical NO₂ profile shapes (Fig. 8d–f, Table A3) and highlights the need for approaches to address the issue. Moreover, improved accuracy in other retrieval parameters, both surface and atmospheric, helps enhance the quality of satellite NO₂ retrievals (Laughner et al., 2019; Vasilkov et al., 2017, 2018; Lorente et al., 2018; Lin et al., 2014, 2015; Liu et al., 2019; Noguchi et al., 2014; Zhou et al., 2011)

4 Conclusions

We conducted a comprehensive intercomparison among various NO₂ measurements made during the five field deployments of DISCOVER-AQ and KORUS-AQ. The field campaigns were conducted in four US states (Maryland, California, Texas, and Colorado) and South Korea. The analyzed datasets were obtained from surface monitors, the NCAR and TD-LIF airborne instruments, ground-based Pandora instruments, and the space-based OMI. We investigated the data from 23 sites among the five campaigns when measurements from all these instruments were available. We focused on an analysis of tropospheric NO₂ column amounts. NO₂ mixing ratio measurements from the surface monitors and airborne instruments were merged and integrated to yield tropospheric columns, while the Pandora tropospheric columns were obtained by subtracting the OMI stratospheric column from Pandora total column observations.

In order to compare OMI NO₂ tropospheric columns with the available validation measurements, we used a combination of observed and simulated NO₂ vertical profiles to recalculate tropospheric NO₂ columns using the OMI Standard Product (OMNO2) version 3.1. To overcome the challenge of comparing OMI NO₂ with its relatively large pixel size to the airborne and ground-based measurements with small spatial scales, we additionally applied a downscaling technique, whereby OMI tropospheric NO₂ columns for each ground pixel are downscaled using high-resolution CMAQ (DISCOVER-AQ) or WRF-Chem (KORUS-AQ) model simulations. Therefore, the comparisons here include three kinds of OMI NO₂ tropospheric columns: (1) OMI Standard Product, (2) OMI data recalculated using observed NO₂ profiles, and (3) downscaled OMI NO₂ data.

The tropospheric columns from the NCAR and TD-LIF airborne instruments generally show good agreement, with a mean difference of 8.4 % and correlation coefficients in the 0.87–0.99 range. The Pandora columns also agree variably with the two airborne instruments, with the campaign-average difference in the range of 3 % to 54 %, but the correlation is not as good ($r = 0.18$ – 0.95) as between the two airborne instruments themselves. There are differences among the campaigns. In particular, all three instruments show the largest discrepancies in the TX campaign; TD-LIF is higher than NCAR by ~ 31.9 %, and Pandora data are lower by ~ 39 % and ~ 54 % compared to NCAR and TD-LIF measurements, respectively.

All three OMI NO₂ columns (Standard Product, based on observed NO₂ profiles, and downscaled) exhibit good correlation with the airborne and ground-based measurements. In terms of quantitative agreement, the OMI SP column is smaller than airborne and ground-based measurements. Retrievals using observed NO₂ profiles bring the OMI column closer to validation measurements. Applying downscaling to OMI data provides further improvement in agreement but little or insignificant change in correlation, perhaps due to the use of model simulations for downscaling.

As discussed in Sect. 3.3, disagreement between the comparatively large OMI pixel and smaller-scale ground and aircraft measurements is to be expected due to the large spatial variability of NO₂. Techniques such as the downscaling method shown here can reduce this discrepancy. However, the robust evaluation of NO₂ tropospheric column retrievals is further confounded by the current lack of agreement among ground-based and in-situ measurements. Future validation strategies for satellite observations of tropospheric column NO₂ will need to address these differences.

Acknowledgements.

The work was supported by NASA's Earth Science Division through Aura Science team and Atmospheric Composition Modeling and Analysis Program (ACMAP) grants. The Dutch-Finnish-built OMI is part of the NASA EOS Aura satellite payload. The OMI is managed by KNMI and the Netherlands Agency for Aerospace Programs (NIVR). NCAR is sponsored by the National Science Foundation (NSF). Pablo E. Saide would like to acknowledge support from NASA grant NNX11AI52G. The authors thank all principal investigators and their staff for providing ground- and aircraft-based NO₂ measurements during the DISCOVER-AQ and KORUS-AQ campaigns.

Financial support.

This research has been supported by the National Aeronautics and Space Administration, Goddard Space Flight Center (grant no. 80NSSC17K0676).

APPENDIX a

Table A1.
Model options for each simulation.

Note that all model options listed are for the domain used for the analysis.

	MD	CA	TX	CO	Korea
Dates	5/24/2011–8/1/2011	1/10/2013–2/28/2013	8/18/2013–10/1/2013	7/9/2014–08/20/2014	5/1/2016–5/31/2016
WRF model options					
Version	3.3	3.8	3.6.1	3.8.1	3.6.1
Model top	100hPa	50hPa	50hPa	50hPa	50hPa
Spatial resolution	4 km	4 km	4 km	4 km	4 km
Vertical levels	34	35	45	37	52
Radiation	LW: RRTM SW: Goddard	LW: RRTMG SW: RRTMG	LW: RRTM SW: Goddard	LW: RRTMG SW: RRTMG	LW: RRTM SW: Goddard
Land surface model	Noah Land Surface Model (Tewari et al., 2004)	Pleim-Xiu (Pleim and Xiu, 2003)	Pleim-Xiu (Pleim and Xiu, 2003)	Unified Noah Land Surface Model	Unified Noah Land Surface Model
Boundary layer	YSU (Hong et al., 2006)	ACM2 (Pleim, 2007)	ACM2 (Pleim, 2007)	YSU (Hong et al., 2006)	MJY scheme
Meteor. init. and bound. cond.	12 km NAM	12 km NAM	12 km NAM	NCAR ECMWF	0.25 degree GFS
CMAQ model options					WRF-Chem
Version	5.0	5.2	5.0.2	5.2 beta	3.6.1 (modified)
Coupled?	No	Yes	No	No	Yes
Chemical mechanism	Carbon Bond (CB05) (Yarwood et al., 2005)	Carbon Bond (CB06, e51)	Carbon Bond (CB05) (Yarwood et al., 2005)	Carbon Bond (CB06, r3)	Reduced hydrocarbon (Pfister et al., 2014)
Aerosol	AE5	AERO6	AE5	AERO6	MOSAIC 4 bin
Chem. init. and bound. cond.	12 km CMAQ v5.0 simulation	12kmCMAQv5.2 simulation	MOZART (outer domain)	RAQMS (outer domain)	24 km MACC for chemistry
Emissions	Described in Loughner et al. (2014)	4 km 2013 emissions, based on the 2011 NEI with year-specific updates to EGU point sources (CEMs data), fires and mobile (MOBILE6)	2012 TCEQ anthropogenic emissions Biogenic Emission Inventory System (BEIS) calculated within CMAQ	Described in report	Described in Goldberg et al. (2019) and Saide et al. (2019)

LW: longwave, SW: shortwave, RRTM: Rapid Radiative Transfer Model, RRTMG: Rapid Radiative Transfer Model for General Circulation Models, AE5: aerosols with aqueous extensions version 5, MOZART: Model for OZone and Related chemical Tracers, RAQMS: Real Time Air Quality Monitoring System, MACC: Monitoring Atmospheric Composition and Climate.

¹ https://www.colorado.gov/airquality/tech_doc_repository.aspx?action=open&file=FRAPPE-NCAR_Final_Report_July2017.pdf (last access: 5 September 2019).

Table A2.
Summary of NO₂ comparison between the OMI Standard Product (OMISP) and NCAR, TD-LIF, and Pandora observations.

The mean difference is calculated as OMI minus observations.

Campaign No. profs (Pandora)	NCAR vs. OMISP		TD-LIF vs. OMISP		Pandora vs. OMISP	
	Mean diff. (%)	<i>r</i>	Mean diff. (%)	<i>r</i>	Mean diff. (%)	<i>r</i>
MD 21 (14)	-40.7	0.39	-34.4	0.54	-21.8	0.21
CA 25 (22)	-53.8	0.77	-56.9	0.81	-58.5	0.24
TX 28 (26)	-54.9	0.65	-65.8	0.56	-26.9	0.65
CO 26 (21)	-67.5	0.73	-65.2	0.75	-68.2	0.72
Korea 11 (5)	-41.9	0.87	-47.9	0.87	-60.1	0.8
All 111 (88)	-51.9	0.82	-55.6	0.83	-54.6	0.84

Table A3.

Same as A2, but for OMI using AMFobs (OMIobs).

Campaign No. profs (Pandora)	NCAR vs. OMISP		TD-LIF vs. OMISP		Pandora vs. OMISP	
	Mean diff. (%)	<i>r</i>	Mean diff. (%)	<i>r</i>	Mean diff. (%)	<i>r</i>
MD21(14)	-23.7	0.61	-17.6	0.7	2.4	0.3
CA 25 (22)	-42.4	0.73	-45.8	0.75	-47.9	0.2
TX 28 (26)	-25.5	0.82	-41.3	0.76	21.6	0.81
CO 26 (21)	-54.2	0.7	-50.5	0.71	-55.2	0.69
Korea 11 (5)	-33.9	0.87	-39.2	0.86	-53.3	0.79
All 111 (88)	-37.5	0.82	-41.5	0.82	-39.2	0.84

Table A4.

Same as A2, but for OMIobs with downscaling (OMIDS).

Campaign No. profs (Pandora)	NCAR vs. OMISP		TD-LIF vs. OMISP		Pandora vs. OMISP	
	Mean diff. (%)	<i>r</i>	Mean diff. (%)	<i>r</i>	Mean diff. (%)	<i>r</i>
MD21 (14)	-24.1	0.75	-18.0	0.85	0.8	0.31
CA 25 (22)	14.2	0.47	7.6	0.56	4.6	0.22
TX 28 (26)	9.5	0.94	-13.8	0.91	78.3	0.93
CO 26 (21)	-42.4	0.7	-37.7	0.71	-42.4	0.67
Korea 11 (5)	-32.8	0.73	-38.4	0.73	-52.1	0.48
All 111 (88)	-12.5	0.65	-18.0	0.68	-12.3	0.57

References

- Anderson DC, Loughner CP, Diskin G, Weinheimer A, Canty TP, Salawitch RJ, Worden HM, Fried A, Mikoviny T, Wisthaler A, and Dickerson RR: Measured and modeled CO and NO_y in DISCOVER-AQ: An evaluation of emissions and chemistry over the eastern US, *Atmos. Environ*, 96, 78–87, 10.1016/j.atmosenv.2014.07.004, 2014.
- Bechle MJ, Millet DB, and Marshall JD: Remote sensing of exposure to NO₂: Satellite versus ground-based measurement in a large urban area, *Atmos. Environ*, 69, 345–353, 10.1016/j.atmosenv.2012.11.046, 2013.
- Beirle S, Platt U, Wenig M, and Wagner T: Weekly cycle of NO₂ by GOME measurements: a signature of anthropogenic sources, *Atmos. Chem. Phys*, 3, 2225–2232, 10.5194/acp-3-2225-2003, 2003.
- Beirle S, Boersma KF, Platt U, Lawrence MG, and Wagner T: Megacity emissions and lifetimes of nitrogen oxides probed from space, *Science*, 333, 1737–1739, 10.1126/science.1207824, 2011. [PubMed: 21940891]
- Boersma KF, Jacob DJ, Bucselo EJ, Perring AE, Dirksen R, van der ARJ, Yantosca RM, Park RJ, Wenig MO, Bertram TH, and Cohen RC: Validation of OMI tropospheric NO₂ Observations During INTEX-B and application to constrain NO_x emissions over the eastern United States and Mexico, *Atmos. Environ*, 42, 4480–4497, 10.1016/j.atmosenv.2008.02.004, 2008.
- Brion J, Chakir A, Daumont D, Malicet J, and Parisse C: High-resolution laboratory absorption cross section of O₃. Temperature effect, *Chem. Phys. Lett*, 213, 610–612, 10.1016/0009-2614(93)89169-I, 1993.
- Bucselo EJ, Celarier EA, Wenig MO, Gleason JF, Veefkind JP, Boersma KF, and Brinksma EJ: Algorithm for NO₂ vertical column retrieval from the ozone monitoring instrument, *IEEE T. Geosci. Remote*, 44, 1245–1258, 10.1109/TGRS.2005.863715, 2006.
- Bucselo EJ, Perring AE, Cohen RC, Boersma KF, Celarier EA, Gleason JF, Wenig MO, Bertram TH, Wooldridge PJ, Dirksen R, and Veefkind JP: Comparison of tropospheric NO₂ from in situ aircraft measurements with near-real-time and standard product data from OMI, *J. Geophys. Res.-Atmos*, 113, D16S31, 10.1029/2007JD008838, 2008.
- Bucselo EJ, Pickering KE, Huntemann TL, Cohen RC, Perring A, Gleason JF, Blakeslee RJ, Albrecht RI, Holzworth R, Cipriani JP, Vargas-Navarro D, Mora-Segura I, Pacheco-Hernández A, and Laporte-Molina S: Lightning-generated NO_x seen by the Ozone Monitoring Instrument during NASA's Tropical Composition, Cloud and Climate Coupling Experiment (TC4), *J. Geophys. Res.-Atmos*, 115, D00J10, 10.1029/2009JD013118, 2010.
- Bucselo EJ, Krotkov NA, Celarier EA, Lamsal LN, Swartz WH, Bhartia PK, Boersma KF, Veefkind JP, Gleason JF, and Pickering KE: A new stratospheric and tropospheric NO₂ retrieval algorithm for nadir-viewing satellite instruments: applications to OMI, *Atmos. Meas. Tech*, 6, 2607–2626, 10.5194/amt-6-2607-2013, 2013.
- Burkholder J, Sander S, Abbatt J, Barker J, Huie R, Kolb C, Kurylo M, Orkin V, Wilmouth D, and Wine P: Chemical Kinetics and Photochemical Data for Use in Atmospheric Studies: Evaluation Number 18, Tech. rep, JPL Publication 15–10, Pasadena, California, USA, 2015.
- Byun D and Schere K: Review of the Governing Equations, Computational Algorithms and Other Components of the Models-3 Community Multiscale Air Quality (CMAQ) Modeling System, *Appl. Mech. Rev*, 59, 51–78, 2005.
- Celarier EA, Brinksma EJ, Gleason JF, Veefkind JP, Cede A, Herman JR, Ionov D, Goutail F, Pommereau J-P, Lambert J-C, Roozendael M. v., Pinardi G, Wittrock F, Schönhardt A, Richter A, Ibrahim OW, Wagner T, Bojkov B, Mount G, Spinei E, Chen CM, Pongetti TJ, Sander SP, Bucselo EJ, Wenig MO, Swart DPJ, Volten H, Kroon M, and Levelt PF: Validation of Ozone Monitoring Instrument nitrogen dioxide columns, *J. Geophys. Res.-Atmos*, 113, D15S15, 10.1029/2007JD008908, 2008.
- Chin M, Diehl T, Tan Q, Prospero JM, Kahn RA, Remer LA, Yu H, Sayer AM, Bian H, Geogdzhayev IV, Holben BN, Howell SG, Huebert BJ, Hsu NC, Kim D, Kucsera TL, Levy RC, Mishchenko MI, Pan X, Quinn PK, Schuster GL, Streets DG, Strode SA, Torres O, and Zhao X-P: Multi-decadal aerosol variations from 1980 to 2009: a perspective from observations and a global model, *Atmos. Chem. Phys*, 14, 3657–3690, 10.5194/acp-14-3657-2014, 2014.

- Cooper M, Martin RV, Padmanabhan A, and Henze DK: Comparing mass balance and adjoint methods for inverse modeling of nitrogen dioxide columns for global nitrogen oxide emissions, *J. Geophys. Res.-Atmos*, 122, 4718–4734, 10.1002/2016JD025985, 2017.
- Dave JV: Importance of higher order scattering in a molecular atmosphere, *J. Opt. Soc. Am*, 54, 307–315, 10.1364/JOSA.54.000307, 1964.
- DeLand M and Marchenko S: The solar chromospheric Ca and Mg indices from Aura OMI, *J. Geophys. Res.-Atmos*, 118, 3415–3423, 10.1002/jgrd.50310, 2013.
- de Wildt MDR, Eskes H, and Boersma KF: The global economic cycle and satellite-derived NO₂ trends over shipping lanes, *Geophys. Res. Lett*, 39, L01802, 10.1029/2011GL049541, 2012.
- Dickerson RR, Anderson DC, and Ren X: On the use of data from commercial NO_x analyzers for air pollution studies, *Atmos. Environ*, 214, 116873, 10.1016/j.atmosenv.2019.116873, 2019.
- DISCOVER-AQ Science Team: DISCOVER-AQ P-3B aircraft in-situ trace gas measurements version 1 – ICARTT File, NASA Langley Atmospheric Science Data Center DAAC, 10.5067/AIRCRAFT/DISCOVER-AQ/AEROSOL-TRACEGAS, 2014.
- Dobber M, Kleipool Q, Dirksen R, Levelt P, Jaross G, Taylor S, Kelly T, Flynn L, Leppelmeier G, and Rozemeijer N: Validation of Ozone Monitoring Instrument level 1b data products, *J. Geophys. Res.-Atmos*, 113, D15S06, 10.1029/2007JD008665, 2008.
- Duncan BN, Strahan SE, Yoshida Y, Steenrod SD, and Livesey N: Model study of the cross-tropopause transport of biomass burning pollution, *Atmos. Chem. Phys*, 7, 3713–3736, 10.5194/acp-7-3713-2007, 2007.
- Duncan BN, Yoshida Y, de Foy B, Lamsal LN, Streets DG, Lu Z, Pickering KE, and Krotkov NA: The observed response of Ozone Monitoring Instrument (OMI) NO₂ columns to NO_x emission controls on power plants in the United States: 2005–2011, *Atmos. Environ*, 81, 102–111, 10.1016/j.atmosenv.2013.08.068, 2013.
- Dunlea EJ, Herndon SC, Nelson DD, Volkamer RM, San Martini F, Sheehy PM, Zahniser MS, Shorter JH, Wormhoudt JC, Lamb BK, Allwine EJ, Gaffney JS, Marley NA, Grutter M, Marquez C, Blanco S, Cardenas B, Retama A, Ramos Villegas CR, Kolb CE, Molina LT, and Molina MJ: Evaluation of nitrogen dioxide chemiluminescence monitors in a polluted urban environment, *Atmos. Chem. Phys*, 7, 2691–2704, 10.5194/acp-7-2691-2007, 2007.
- Fehsenfeld FC, Drummond JW, Roychowdhury UK, Galvin PJ, Williams EJ, Buhr MP, Parrish DD, Hübler G, Langford AO, Calvert JG, Ridley BA, Grahek F, Heikes BG, Kok GL, Shetter JD, Walega JG, Elsworth CM, Norton RB, Fahey DW, Murphy PC, Hovermale C, Mohnen VA, Demerjian KL, Mackay GI, and Schiff HI: Intercomparison of NO₂ measurement techniques, *J. Geophys. Res.-Atmos*, 95, 3579–3597, 10.1029/JD095iD04p03579, 1990.
- Geddes JA and Martin RV: Global deposition of total reactive nitrogen oxides from 1996 to 2014 constrained with satellite observations of NO₂ columns, *Atmos. Chem. Phys*, 17, 10071–10091, 10.5194/acp-17-10071-2017, 2017.
- Gelaro R, McCarty W, Suárez MJ, Todling R, Molod A, Takacs L, Randles CA, Darmenov A, Bosilovich MG, Reichle R, Wargan K, Coy L, Cullather R, Draper C, Akella S, Buchard V, Conaty A, da Silva AM, Gu W, Kim G-K, Koster R, Lucchesi R, Merkova D, Nielsen JE, Partyka G, Pawson S, Putman W, Rienecker M, Schubert SD, Sienkiewicz M, and Zhao B: The Modern-Era Retrospective Analysis for Research and Applications, Version 2 (MERRA-2), *J. Climate*, 30, 5419–5454, 10.1175/JCLI-D-16-0758.1, 2017.
- Ghude SD, Lal DM, Beig G, van der AR, and Sable D: Rain-Induced Soil NO_x Emission From India During the Onset of the Summer Monsoon: A Satellite Perspective, *J. Geophys. Res.-Atmos*, 115, D16304, 10.1029/2009JD013367, 2010.
- Ghude SD, Kulkarni SH, Jena C, Pfister GG, Beig G, Fadnavis S, and van der ARJ: Application of satellite observations for identifying regions of dominant sources of nitrogen oxides over the Indian Subcontinent, *J. Geophys. Res.-Atmos*, 118, 1075–1089, 10.1029/2012JD017811, 2013a.
- Ghude SD, Pfister GG, Jena C, A R. J. v. d, Emmons LK, and Kumar R: Satellite constraints of nitrogen oxide (NO_x) emissions from India based on OMI observations and WRF-Chem simulations, *Geophys. Res. Lett*, 40, 423–428, 10.1002/grl.50065, 2013b.

- Goldberg DL, Lamsal LN, Loughner CP, Swartz WH, Lu Z, and Streets DG: A high-resolution and observationally constrained OMI NO₂ satellite retrieval, *Atmos. Chem. Phys.*, 17, 11403–11421, 10.5194/acp-17-11403-2017, 2017.
- Goldberg DL, Saide PE, Lamsal LN, de Foy B, Lu Z, Woo J-H, Kim Y, Kim J, Gao M, Carmichael G, and Streets DG: A top-down assessment using OMI NO₂ suggests an underestimate in the NO_x emissions inventory in Seoul, South Korea, during KORUS-AQ, *Atmos. Chem. Phys.*, 19, 1801–1818, 10.5194/acp-19-1801-2019, 2019.
- Grell GA, Peckham SE, Schmitz R, McKeen SA, Frost G, Skamarock WC, and Eder B: Fully coupled “online” chemistry within the WRF model, *Atmos. Environ.*, 39, 6957–6975, 10.1016/j.atmosenv.2005.04.027, 2005.
- Hains JC, Boersma KF, Kroon M, Dirksen RJ, Cohen RC, Perring AE, Bucsela E, Volten H, Swart DPJ, Richter A, Wittrock F, Schoenhardt A, Wagner T, Ibrahim OW, Roozendael M. v., Pinardi G, Gleason JF, Veeffkind JP, and Levelt P: Testing and improving OMI DOMINO tropospheric NO₂ using observations from the DANDELIONS and INTEX-B validation campaigns, *J. Geophys. Res.-Atmos.*, 115, D05301, 10.1029/2009JD012399, 2010.
- Herman J, Cede A, Spinei E, Mount G, Tzortziou M, and Abuhassan N: NO₂ column amounts from ground-based Pandora and MFDOAS spectrometers using the direct-sun DOAS technique: Intercomparisons and application to OMI validation, *J. Geophys. Res.-Atmos.*, 114, D13307, 10.1029/2009JD011848, 2009.
- Herman J, Spinei E, Fried A, Kim J, Kim J, Kim W, Cede A, Abuhassan N, and Segal-Rozenhaimer M: NO₂ and HCHO measurements in Korea from 2012 to 2016 from Pandora spectrometer instruments compared with OMI retrievals and with aircraft measurements during the KORUS-AQ campaign, *Atmos. Meas. Tech.*, 11, 4583–4603, 10.5194/amt-11-4583-2018, 2018.
- Herron-Thorpe FL, Lamb BK, Mount GH, and Vaughan JK: Evaluation of a regional air quality forecast model for tropospheric NO₂ columns using the OMI/Aura satellite tropospheric NO₂ product, *Atmos. Chem. Phys.*, 10, 8839–8854, 10.5194/acp-10-8839-2010, 2010.
- Hilboll A, Richter A, and Burrows JP: Long-term changes of tropospheric NO₂ over megacities derived from multiple satellite instruments, *Atmos. Chem. Phys.*, 13, 4145–4169, 10.5194/acp-13-4145-2013, 2013.
- Hong S-Y, Noh Y, and Dudhia J: A new vertical diffusion package with an explicit treatment of entrainment processes, *Mon. Weather Rev.*, 134, 2318–2341, 10.1175/MWR3199.1, 2006.
- Huijnen V, Eskes HJ, Poupkou A, Elbern H, Boersma KF, Foret G, Sofiev M, Valdebenito A, Flemming J, Stein O, Gross A, Robertson L, D’Isidoro M, Kioutsioukis I, Friese E, Amstrup B, Bergstrom R, Strunk A, Vira J, Zyryanov D, Maurizi A, Melas D, Peuch V-H, and Zerefos C: Comparison of OMI NO₂ tropospheric columns with an ensemble of global and European regional air quality models, *Atmos. Chem. Phys.*, 10, 3273–3296, 10.5194/acp-10-3273-2010, 2010.
- Ialongo I, Herman J, Krotkov N, Lamsal L, Boersma KF, Hovila J, and Tamminen J: Comparison of OMI NO₂ observations and their seasonal and weekly cycles with ground-based measurements in Helsinki, *Atmos. Meas. Tech.*, 9, 5203–5212, 10.5194/amt-9-5203-2016, 2016.
- Irie H, Boersma KF, Kanaya Y, Takashima H, Pan X, and Wang ZF: Quantitative bias estimates for tropospheric NO₂ columns retrieved from SCIAMACHY, OMI, and GOME-2 using a common standard for East Asia, *Atmos. Meas. Tech.*, 5, 2403–2411, 10.5194/amt-5-2403-2012, 2012.
- Jaeglé L, Steinberger L, Martin RV, and Chance K: Global partitioning of NO_x sources using satellite observations: Relative roles of fossil fuel combustion, biomass burning and soil emissions, *Faraday Discuss.*, 130, 407–423, 10.1039/B502128F, 2005. [PubMed: 16161795]
- Judd LM, Al-Saadi JA, Janz SJ, Kowalewski MG, Pierce RB, Szykman JJ, Valin LC, Swap R, Cede A, Mueller M, Tiefengraber M, Abuhassan N, and Williams D: Evaluating the impact of spatial resolution on tropospheric NO₂ column comparisons within urban areas using high-resolution airborne data, *Atmos. Meas. Tech.*, 12, 6091–6111, 10.5194/amt-12-6091-2019, 2019.
- Kebabian PL, Wood EC, Herndon SC, and Freedman A: A practical alternative to chemiluminescence-based detection of nitrogen dioxide: cavity attenuated phase shift spectroscopy, *Environ. Sci. Technol.*, 42, 6040–6045, 10.1021/es703204j, 2008. [PubMed: 18767663]
- Kim HC, Lee P, Judd L, Pan L, and Lefer B: OMI NO₂ column densities over North American urban cities: the effect of satellite footprint resolution, *Geosci. Model Dev.*, 9, 1111–1123, 10.5194/gmd-9-1111-2016, 2016.

- Kim HC, Lee S-M, Chai T, Ngan F, Pan L, and Lee P: A conservative downscaling of satellite-detected chemical compositions: NO₂ column densities of OMI, GOME-2, and CMAQ, *Remote Sensing*, 10, 1001, 10.3390/rs10071001, 2018.
- Kim S-W, Heckel A, Frost GJ, Richter A, Gleason J, Burrows JP, McKeen S, Hsie E-Y, Granier C, and Trainer M: NO₂ columns in the western United States observed from space and simulated by a regional chemistry model and their implications for NO_x emissions, *J. Geophys. Res.-Atmos*, 114, D11301, 10.1029/2008JD011343, 2009.
- Konovalov IB, Beekmann M, Richter A, and Burrows JP: Inverse modelling of the spatial distribution of NO_x emissions on a continental scale using satellite data, *Atmos. Chem. Phys.*, 6, 1747–1770, 10.5194/acp-6-1747-2006, 2006.
- KORUS-AQ Science Team: KORUS-AQ airborne mission in-situ trace gas measurements version 1 – ICARTT File, NASA Langley Atmospheric Science Data Center DAAC, 10.5067/Suborbital/KORUS-AQ/DATA01, 2018.
- Krotkov NA, McLinden CA, Li C, Lamsal LN, Celarier EA, Marchenko SV, Swartz WH, Bucsela EJ, Joiner J, Duncan BN, Boersma KF, Veefkind JP, Levelt PF, Fioletov VE, Dickerson RR, He H, Lu Z, and Streets DG: Aura OMI observations of regional SO₂ and NO₂ pollution changes from 2005 to 2015, *Atmos. Chem. Phys.*, 16, 4605–4629, 10.5194/acp-16-4605-2016, 2016.
- Krotkov NA, Lamsal LN, Celarier EA, Swartz WH, Marchenko SV, Bucsela EJ, Chan KL, Wenig M, and Zara M: The version 3 OMI NO₂ standard product, *Atmos. Meas. Tech.*, 10, 3133–3149, 10.5194/amt-10-3133-2017, 2017.
- Krotkov NA, Lamsal LN, Marchenko SV, Celarier EA, Bucsela EJ, Swartz WH, Joiner J, and the OMI core team: OMI/Aura nitrogen dioxide (NO₂) total and tropospheric column 1-orbit L2 swath 13×24 km V003, Greenbelt, MD, USA, Goddard Earth Sciences Data and Information Services Center (GES DISC), 10.5067/Aura/OMI/DATA2017, 2019 OMI/Aura Nitrogen Dioxide (NO₂) Total and Tropospheric Column 1-orbit L2 Swath 13×24 km V003, Greenbelt, MD, USA, Goddard Earth Sciences Data and Information Services Center (GES DISC), 10.5067/Aura/OMI/DATA2017, 2019.
- Lamsal LN, Martin RV, Donkelaar AV, Steinbacher M, Celarier EA, Bucsela E, Dunlea EJ, and Pinto JP: Ground-level nitrogen dioxide concentrations inferred from the satellite-borne Ozone Monitoring Instrument, *J. Geophys. Res.-Atmos*, 113, D16308, 10.1029/2007JD009235, 2008.
- Lamsal LN, Martin RV, Donkelaar A. v., Celarier EA, Bucsela EJ, Boersma KF, Dirksen R, Luo C, and Wang Y: Indirect validation of tropospheric nitrogen dioxide retrieved from the OMI satellite instrument: Insight into the seasonal variation of nitrogen oxides at northern midlatitudes, *J. Geophys. Res.-Atmos*, 115, D05302, 10.1029/2009JD013351, 2010.
- Lamsal LN, Martin RV, Padmanabhan A, van Donkelaar A, Zhang Q, Sioris CE, Chance K, Kurosu TP, and Newchurch MJ: Application of satellite observations for timely updates to global anthropogenic NO_x emission inventories, *Geophys. Res. Lett.*, 38, L05810, 10.1029/2010GL046476, 2011.
- Lamsal LN, Krotkov NA, Celarier EA, Swartz WH, Pickering KE, Bucsela EJ, Gleason JF, Martin RV, Philip S, Irie H, Cede A, Herman J, Weinheimer A, Szykman JJ, and Knepp TN: Evaluation of OMI operational standard NO₂ column retrievals using in situ and surface-based NO₂ observations, *Atmos. Chem. Phys.*, 14, 11587–11609, 10.5194/acp-14-11587-2014, 2014.
- Lamsal LN, Duncan BN, Yoshida Y, Krotkov NA, Pickering KE, Streets DG, and Lu Z: U.S. NO₂ trends (2005–2013): EPA Air Quality System (AQS) data versus improved observations from the Ozone Monitoring Instrument (OMI), *Atmos. Environ.*, 110, 130–143, 10.1016/j.atmosenv.2015.03.055, 2015.
- Lamsal LN, Janz SJ, Krotkov NA, Pickering KE, Spurr RJD, Kowalewski MG, Loughner CP, Crawford JH, Swartz WH, and Herman JR: High-resolution NO₂ observations from the Airborne Compact Atmospheric Mapper: retrieval and validation, *J. Geophys. Res.-Atmos*, 122, 1953–1970, 10.1002/2016JD025483, 2017.
- Laughner JL, Zare A, and Cohen RC: Effects of daily meteorology on the interpretation of space-based remote sensing of NO₂, *Atmos. Chem. Phys.*, 16, 15247–15264, 10.5194/acp-16-15247-2016, 2016.
- Laughner JL, Zhu Q, and Cohen RC: Evaluation of version 3.0B of the BEHR OMI NO₂ product, *Atmos. Meas. Tech.*, 12, 129–146, 10.5194/amt-12-129-2019, 2019.

- Levelt PF, Oord GHJ, v. d., Dobber MR, Malkki A, Huib Visser, Johan de Vries, Stammes P, Lundell JOV, and Saari H: The ozone monitoring instrument, *IEEE T. Geosci. Remote*, 44, 1093–1101, 10.1109/TGRS.2006.872333, 2006.
- Levelt PF, Joiner J, Tamminen J, Veefkind JP, Bhartia PK, Stein Zweers DC, Duncan BN, Streets DG, Eskes H, van der AR, McLinden C, Fioletov V, Carn S, de Laat J, DeLand M, Marchenko S, McPeters R, Ziemke J, Fu D, Liu X, Pickering K, Apituley A, González Abad G, Arola A, Boersma F, Chan Miller C, Chance K, de Graaf M, Hakkarainen J, Hassinen S, Ialongo I, Kleipool Q, Krotkov N, Li C, Lamsal L, Newman P, Nowlan C, Suleiman R, Tilstra LG, Torres O, Wang H, and Wargan K: The Ozone Monitoring Instrument: overview of 14 years in space, *Atmos. Chem. Phys.*, 18, 5699–5745, 10.5194/acp-18-5699-2018, 2018.
- Lin J-T: Satellite constraint for emissions of nitrogen oxides from anthropogenic, lightning and soil sources over East China on a high-resolution grid, *Atmos. Chem. Phys.*, 12, 2881–2898, 10.5194/acp-12-2881-2012, 2012.
- Lin J-T, McElroy MB, and Boersma KF: Constraint of anthropogenic NO_x emissions in China from different sectors: a new methodology using multiple satellite retrievals, *Atmos. Chem. Phys.*, 10, 63–78, 10.5194/acp-10-63-2010, 2010.
- Lin J-T, Martin RV, Boersma KF, Sneep M, Stammes P, Spurr R, Wang P, Van Roozendael M, Clémer K, and Irie H: Retrieving tropospheric nitrogen dioxide from the Ozone Monitoring Instrument: effects of aerosols, surface reflectance anisotropy, and vertical profile of nitrogen dioxide, *Atmos. Chem. Phys.*, 14, 1441–1461, 10.5194/acp-14-1441-2014, 2014.
- Lin J-T, Liu M-Y, Xin J-Y, Boersma KF, Spurr R, Martin R, and Zhang Q: Influence of aerosols and surface reflectance on satellite NO₂ retrieval: seasonal and spatial characteristics and implications for NO_x emission constraints, *Atmos. Chem. Phys.*, 15, 11217–11241, 10.5194/acp-15-11217-2015, 2015.
- Liu F, van der ARJ, Eskes H, Ding J, and Mijling B: Evaluation of modeling NO₂ concentrations driven by satellite-derived and bottom-up emission inventories using in situ measurements over China, *Atmos. Chem. Phys.*, 18, 4171–4186, 10.5194/acp-18-4171-2018, 2018.
- Liu M, Lin J, Boersma KF, Pinardi G, Wang Y, Chimot J, Wagner T, Xie P, Eskes H, Van Roozendael M, Hendrick F, Wang P, Wang T, Yan Y, Chen L, and Ni R: Improved aerosol correction for OMI tropospheric NO₂ retrieval over East Asia: constraint from CALIOP aerosol vertical profile, *Atmos. Meas. Tech.*, 12, 1–21, 10.5194/amt-12-1-2019, 2019.
- Lorente A, Boersma KF, Stammes P, Tilstra LG, Richter A, Yu H, Kharbouche S, and Muller J-P: The importance of surface reflectance anisotropy for cloud and NO₂ retrievals from GOME-2 and OMI, *Atmos. Meas. Tech.*, 11, 4509–4529, 10.5194/amt-11-4509-2018, 2018.
- Loughner CP, Tzortziou M, Follette-Cook M, Pickering KE, Goldberg D, Satam C, Weinheimer A, Crawford JH, Knapp DJ, Montzka DD, Diskin GS, and Dickerson RR: Impact of bay-breeze circulations on surface air quality and boundary layer export, *J. Appl. Meteorol. Clim.*, 53, 1697–1713, 10.1175/JAMC-D-13-0323.1, 2014.
- Lu Z and Streets DG: Increase in NO_x emissions from Indian thermal power plants during 1996–2010: unit-based inventories and multisatellite observations, *Environ. Sci. Technol.*, 46, 7463–7470, 10.1021/es300831w, 2012. [PubMed: 22732062]
- Marchenko S, Krotkov NA, Lamsal LN, Celarier EA, Swartz WH, and Bucsela EJ: Revising the slant column density retrieval of nitrogen dioxide observed by the Ozone Monitoring Instrument, *J. Geophys. Res.-Atmos.*, 120, 5670–5692, 10.1002/2014JD022913, 2015. [PubMed: 27708989]
- Martin RV, Chance K, Jacob DJ, Kurosu TP, Spurr RJD, Bucsela E, Gleason JF, Palmer PI, Bey I, Fiore AM, Li Q, Yantosca RM, and Koelemeijer RBA: An improved retrieval of tropospheric nitrogen dioxide from GOME, *J. Geophys. Res.-Atmos.*, 107, ACH 9–1–ACH 9–21, 10.1029/2001JD001027, 2002.
- Martin RV, Jacob DJ, Chance K, Kurosu TP, Palmer PI, and Evans MJ: Global inventory of nitrogen oxide emissions constrained by space-based observations of NO₂ columns, *J. Geophys. Res.-Atmos.*, 108, 4537, 10.1029/2003JD003453, 2003.
- McLinden CA, Fioletov V, Boersma KF, Kharol SK, Krotkov N, Lamsal L, Makar PA, Martin RV, Veefkind JP, and Yang K: Improved satellite retrievals of NO₂ and SO₂ over the Canadian oil sands and comparisons with surface measurements, *Atmos. Chem. Phys.*, 14, 3637–3656, 10.5194/acp-14-3637-2014, 2014.

- Mebust AK and Cohen RC: Observations of a seasonal cycle in NO_x emissions from fires in African woody savannas, *Geophys. Res. Lett*, 40, 1451–1455, 10.1002/grl.50343, 2013.
- Miyazaki K, Eskes H, Sudo K, Boersma KF, Bowman K, and Kanaya Y: Decadal changes in global surface NO_x emissions from multi-constituent satellite data assimilation, *Atmos. Chem. Phys*, 17, 807–837, 10.5194/acp-17-807-2017, 2017.
- Murray LT, Jacob DJ, Logan JA, Hudman RC, and Koshak WJ: Optimized regional and interannual variability of lightning in a global chemical transport model constrained by LIS/OTD satellite data, *J. Geophys. Res.-Atmos*, 117, D20307, 10.1029/2012JD017934, 2012.
- Murray LT, Mickley LJ, Kaplan JO, Sofen ED, Pfeiffer M, and Alexander B: Factors controlling variability in the oxidative capacity of the troposphere since the Last Glacial Maximum, *Atmos. Chem. Phys*, 14, 3589–3622, 10.5194/acp-14-3589-2014, 2014.
- Noguchi K, Richter A, Rozanov V, Rozanov A, Burrows JP, Irie H, and Kita K: Effect of surface BRDF of various land cover types on geostationary observations of tropospheric NO_2 , *Atmos. Meas. Tech*, 7, 3497–3508, 10.5194/amt-7-3497-2014, 2014.
- Novotny EV, Bechle MJ, Millet DB, and Marshall JD: National satellite-based land-use regression: NO_2 in the United States, *Environ. Sci. Technol*, 45, 4407–4414, 10.1021/es103578x, 2011. [PubMed: 21520942]
- Nowlan CR, Martin RV, Philip S, Lamsal LN, Krotkov NA, Marais EA, Wang S, and Zhang Q: Global dry deposition of nitrogen dioxide and sulfur dioxide inferred from space-based measurements, *Global Biogeochem. Cy*, 28, 1025–1043, 10.1002/2014GB004805, 2014.
- Nowlan CR, Liu X, Leitch JW, Chance K, González Abad G, Liu C, Zoogman P, Cole J, Delker T, Good W, Murcray F, Ruppert L, Soo D, Follette-Cook MB, Janz SJ, Kowalewski MG, Loughner CP, Pickering KE, Herman JR, Beaver MR, Long RW, Szykman JJ, Judd LM, Kelley P, Luke WT, Ren X, and Al-Saadi JA: Nitrogen dioxide observations from the Geostationary Trace gas and Aerosol Sensor Optimization (GeoTASO) airborne instrument: Retrieval algorithm and measurements during DISCOVER-AQ Texas 2013, *Atmos. Meas. Tech*, 9, 2647–2668, 10.5194/amt-9-2647-2016, 2016.
- Nowlan CR, Liu X, Janz SJ, Kowalewski MG, Chance K, Follette-Cook MB, Fried A, González Abad G, Herman JR, Judd LM, Kwon H-A, Loughner CP, Pickering KE, Richter D, Spinei E, Walega J, Weibring P, and Weinheimer AJ: Nitrogen dioxide and formaldehyde measurements from the GEOstationary Coastal and Air Pollution Events (GEO-CAPE) Airborne Simulator over Houston, Texas, *Atmos. Meas. Tech*, 11, 5941–5964, 10.5194/amt-11-5941-2018, 2018.
- Pfister GG, Walters S, Lamarque J-F, Fast J, Barth MC, Wong J, Done J, Holland G, and Bruyère CL: Projections of future summertime ozone over the U.S., *J. Geophys. Res.-Atmos*, 119, 5559–5582, 10.1002/2013JD020932, 2014.
- Pickering KE, Bucsela E, Allen D, Ring A, Holzworth R, and Krotkov N: Estimates of lightning NO_x production based on OMI NO_2 observations over the Gulf of Mexico, *J. Geophys. Res.-Atmos*, 121, 8668–8691, 10.1002/2015JD024179, 2016.
- Platt U: Differential optical absorption spectroscopy (DOAS), in: *Air Monitoring by Spectroscopic Techniques*, edited by: M. W. Sgrist, Chemical Analysis Series, Vol. 127, John Wiley & Sons, Inc., 1994.
- Pleim JE: A Combined Local and Nonlocal Closure Model for the Atmospheric Boundary Layer. Part II: Application and Evaluation in a Mesoscale Meteorological Model, *J. Appl. Meteorol. Clim*, 46, 1396–1409, 10.1175/JAM2534.1, 2007.
- Pleim JE and Xiu A: Development of a Land Surface Model. Part II: Data Assimilation, *J. Appl. Meteorol*, 42, 1811–1822, 10.1175/1520-0450(2003)042<1811:DOALSM>2.0.CO;2, 2003.
- Richter A, Burrows JP, Nüß H, Granier C, and Niemeier U: Increase in tropospheric nitrogen dioxide over China observed from space, *Nature*, 437, 129–132, 10.1038/nature04092, 2005. [PubMed: 16136141]
- Ridley BA and Grahek FE: A small, low flow, high sensitivity reaction vessel for NO chemiluminescence detectors, *J. Atmos. Ocean. Tech*, 7, 307–311, 10.1175/1520-0426(1990)007<0307:ASLFHS>2.0.CO;2, 1990.

- Russell AR, Valin LC, Bucselo EJ, Wenig MO, and Cohen RC: Space-based constraints on spatial and temporal patterns of NO_x emissions in California, 2005–2008, *Environ. Sci. Technol*, 44, 3608–3615, 10.1021/es903451j, 2010. [PubMed: 20364869]
- Russell AR, Valin LC, and Cohen RC: Trends in OMI NO₂ observations over the United States: effects of emission control technology and the economic recession, *Atmos. Chem. Phys*, 12, 12197–12209, 10.5194/acp-12-12197-2012, 2012.
- Ryerson TB, Williams EJ, and Fehsenfeld FC: An efficient photolysis system for fast-response NO₂ measurements, *J. Geophys. Res*, 105, 26447–26461, 10.1029/2000JD900389, 2000.
- Saide PE, Kim J, Song CH, Choi M, Cheng Y, and Carmichael GR: Assimilation of next generation geostationary aerosol optical depth retrievals to improve air quality simulations, *Geophys. Res. Lett*, 41, 9188–9196, 10.1002/2014GL062089, 2014.
- Saide PE, Gao M, Lu Z, Goldberg D, Streets DG, Woo J-H, Beyersdorf A, Corr CA, Thornhill KL, Anderson B, Hair JW, Nehrir AR, Diskin GS, Jimenez JL, Nault BA, Campuzano-Jost P, Dibb J, Heim E, Lamb KD, Schwarz JP, Perring AE, Kim J, Choi M, Holben B, Pfister G, Hodzic A, Carmichael GR, Emmons L, and Crawford JH: Understanding and improving model representation of aerosol optical properties for a Chinese haze event measured during KORUS-AQ, *Atmos. Chem. Phys. Discuss*, 10.5194/acp-2019-1022, in review 2019.
- Schaub D, Brunner D, Boersma KF, Keller J, Folini D, Buchmann B, Berresheim H, and Staehelin J: SCIAMACHY tropospheric NO₂ over Switzerland: estimates of NO_x lifetimes and impact of the complex Alpine topography on the retrieval, *Atmos. Chem. Phys*, 7, 5971–5987, 10.5194/acp-7-5971-2007, 2007.
- Schenkeveld VME, Jaross G, Marchenko S, Haffner D, Kleipool QL, Rozemeijer NC, Veeffkind JP, and Levelt PF: In-flight performance of the Ozone Monitoring Instrument, *Atmos. Meas. Tech*, 10, 1957–1986, 10.5194/amt-10-1957-2017, 2017. [PubMed: 29657582]
- Schreier SF, Richter A, Schepaschenko D, Shvidenko A, Hilboll A, and Burrows JP: Differences in satellite-derived NO_x emission factors between Eurasian and North American boreal forest fires, *Atmos. Environ*, 121, 55–65, 10.1016/j.atmosenv.2014.08.071, 2015.
- Skamarock WC, Klemp JB, Dudhia J, Gill DO, Barker DM, Wang W, and Powers JG: A description of the Advanced Research WRF version 3 NCAR Technical note -475+STR, NCAR, Boulder, Colorado, USA, 2008.
- Sluis WW, Allaart MAF, Pijters AJM, and Gast LFL: The development of a nitrogen dioxide sonde, *Atmos. Meas. Tech*, 3, 1753–1762, 10.5194/amt-3-1753-2010, 2010.
- Spinei E, Cede A, Swartz WH, Herman J, and Mount GH: The use of NO₂ absorption cross section temperature sensitivity to derive NO₂ profile temperature and stratospheric–tropospheric column partitioning from visible direct-sun DOAS measurements, *Atmos. Meas. Tech*, 7, 4299–4316, 10.5194/amt-7-4299-2014, 2014.
- Steinbacher M, Zellweger C, Schwarzenbach B, Bugmann S, Buchmann B, Ordóñez C, Prevot ASH, and Hueglin C: Nitrogen oxide measurements at rural sites in Switzerland: Bias of conventional measurement techniques, *J. Geophys. Res.-Atmos*, 112, D11307, 10.1029/2006JD007971, 2007.
- Strahan SE, Douglass AR, and Newman PA: The contributions of chemistry and transport to low arctic ozone in March 2011 derived from Aura MLS observations, *J. Geophys. Res.-Atmos*, 118, 1563–1576, 10.1002/jgrd.50181, 2013.
- Strahan SE, Douglass AR, and Steenrod SD: Chemical and dynamical impacts of stratospheric sudden warmings on Arctic ozone variability, *J. Geophys. Res.-Atmos*, 121, 11836–11851, 10.1002/2016JD025128, 2016. [PubMed: 29963345]
- Strode SA, Rodriguez JM, Logan JA, Cooper OR, Witte JC, Lamsal LN, Damon M, Aartsen BV, Steenrod SD, and Strahan SE: Trends and variability in surface ozone over the United States, *J. Geophys. Res.-Atmos*, 120, 9020–9042, 10.1002/2014JD022784, 2015.
- Tewari M, Chen F, Wang W, Dudhia J, LeMone M, Mitchell K, Ek M, Gayno G, Wegiel J, and Cuenca R: Implementation and verification of the unified NOAA land surface model in the WRF model, vol. 1115, American Meteorological Society, Seattle, Washington, USA, 2004.
- Thornton JA, Wooldridge PJ, and Cohen RC: Atmospheric NO₂: in situ laser-induced fluorescence detection at parts per trillion mixing ratios, *Anal. Chem*, 72, 528–539, 10.1021/ac9908905, 2000. [PubMed: 10695138]

- Tzortziou M, Herman JR, Cede A, Loughner CP, Abuhassan N, and Naik S: Spatial and temporal variability of ozone and nitrogen dioxide over a major urban estuarine ecosystem, *J. Atmos. Chem.*, 72, 287–309, 10.1007/s10874-013-9255-8, 2015.
- Tzortziou M, Parker O, Lamb B, Herman JR, Lamsal L, Stauffer R, and Abuhassan N: Atmospheric trace gas (NO₂ and O₃) variability in South Korean coastal waters, and implications for remote sensing of coastal ocean color dynamics, *Remote Sensing*, 10, 1587, 10.3390/rs10101587, 2018.
- Valin LC, Russell AR, and Cohen RC: Variations of OH radical in an urban plume inferred from NO₂ column measurements, *Geophys. Res. Lett.*, 40, 1856–1860, 10.1002/grl.50267, 2013.
- van der ARJ, Eskes HJ, Boersma KF, Noije T. P. C. v., Roozendael MV, Smedt ID, Peters DHMU, and Meijer EW: Trends, seasonal variability and dominant NO_x source derived from a ten year record of NO₂ measured from space, *J. Geophys. Res.-Atmos.*, 113, D04302, 10.1029/2007JD009021, 2008.
- van Noije TPC, Eskes HJ, Dentener FJ, Stevenson DS, Ellingsen K, Schultz MG, Wild O, Amann M, Atherton CS, Bergmann DJ, Bey I, Boersma KF, Butler T, Cofala J, Drevet J, Fiore AM, Gauss M, Hauglustaine DA, Horowitz LW, Isaksen ISA, Krol MC, Lamarque J-F, Lawrence MG, Martin RV, Montanaro V, Müller J-F, Pitari G, Prather MJ, Pyle JA, Richter A, Rodriguez JM, Savage NH, Strahan SE, Sudo K, Szopa S, and van Roozendael M: Multi-model ensemble simulations of tropospheric NO₂ compared with GOME retrievals for the year 2000, *Atmos. Chem. Phys.*, 6, 2943–2979, 10.5194/acp-6-2943-2006, 2006.
- Vandaele AC, Hermans C, Simon PC, Carleer M, Colin R, Fally S, Mérienne MF, Jenouvrier A, and Coquart B: Measurements of the NO₂ absorption cross-section from 42 000 cm⁻¹ to 10 000 cm⁻¹ (238–1000 nm) at 220 K and 294 K, *J. Quant. Spectrosc. Ra.*, 59, 171–184, 10.1016/S0022-4073(97)00168-4, 1998.
- Vasilkov A, Qin W, Krotkov N, Lamsal L, Spurr R, Haffner D, Joiner J, Yang E-S, and Marchenko S: Accounting for the effects of surface BRDF on satellite cloud and trace-gas retrievals: a new approach based on geometry-dependent Lambertian equivalent reflectivity applied to OMI algorithms, *Atmos. Meas. Tech.*, 10, 333–349, 10.5194/amt-10-333-2017, 2017.
- Vasilkov A, Yang E-S, Marchenko S, Qin W, Lamsal L, Joiner J, Krotkov N, Haffner D, Bhartia PK, and Spurr R: A cloud algorithm based on the O₂-O₂ 477 nm absorption band featuring an advanced spectral fitting method and the use of surface geometry-dependent Lambertian-equivalent reflectivity, *Atmos. Meas. Tech.*, 11, 4093–4107, 10.5194/amt-11-4093-2018, 2018.
- Veefkind JP, de Haan JF, Sneep M, and Levelt PF: Improvements to the OMI O₂–O₂ operational cloud algorithm and comparisons with ground-based radar–lidar observations, *Atmos. Meas. Tech.*, 9, 6035–6049, 10.5194/amt-9-6035-2016, 2016.
- Vinken GCM, Boersma KF, van Donkelaar A, and Zhang L: Constraints on ship NO_x emissions in Europe using GEOS-Chem and OMI satellite NO₂ observations, *Atmos. Chem. Phys.*, 14, 1353–1369, 10.5194/acp-14-1353-2014, 2014.
- Vlemmix T, PETERS AJM, Stammes P, Wang P, and Levelt PF: Retrieval of tropospheric NO₂ using the MAX-DOAS method combined with relative intensity measurements for aerosol correction, *Atmos. Meas. Tech.*, 3, 1287–1305, 10.5194/amt-3-1287-2010, 2010.
- Wang SW, Zhang Q, Streets DG, He KB, Martin RV, Lamsal LN, Chen D, Lei Y, and Lu Z: Growth in NO_x emissions from power plants in China: bottom-up estimates and satellite observations, *Atmos. Chem. Phys.*, 12, 4429–4447, 10.5194/acp-12-4429-2012, 2012.
- WHO: Review of evidence on health aspects of air pollution REVIHAAP Project, Tech. rep., 302 pp, World Health Organization, Copenhagen, Denmark, available at: http://www.euro.who.int/_data/assets/pdf_file/0004/193108/REVIHAAP-Final-technical-report-final-version.pdf?ua=1 (last access: 5 September 2019), 2013.
- Wild RJ, Edwards PM, Dubé WP, Baumann K, Edgerton ES, Quinn PK, Roberts JM, Rollins AW, Veres PR, Warneke C, Williams EJ, Yuan B, and Brown SS: A measurement of total reactive nitrogen, NO_y, together with NO₂, NO, and O₃ via cavity ring-down spectroscopy, *Environ. Sci. Technol.*, 48, 9609–9615, 10.1021/es501896w, 2014. [PubMed: 25019919]
- Wong DC, Pleim J, Mathur R, Binkowski F, Otte T, Gilliam R, Pouliot G, Xiu A, Young JO, and Kang D: WRF-CMAQ two-way coupled system with aerosol feedback: software development and preliminary results, *Geosci. Model Dev.*, 5, 299–312, 10.5194/gmd-5-299-2012, 2012.

- Yarwood G, Rao S, Yocke M, and Whitten G: Updates to the Carbon Bond Chemical Mechanism: CB05. RT-0400675, vol. 8, U.S Environmental Protection Agency, Washington, District of Columbia, USA, 2005.
- Zhao C and Wang Y: Assimilated inversion of NO_x emissions over east Asia using OMI NO_2 column measurements, *Geophys. Res. Lett.*, 36, L06805, 10.1029/2008GL037123, 2009.
- Zhou DK, Larar AM, Liu X, Smith WL, Strow LL, Yang P, Schlüssel P, and Calbet X: Global Land Surface Emissivity Retrieved From Satellite Ultraspectral IR Measurements, *IEEE T. Geosci. Remote*, 49, 1277–1290, 10.1109/TGRS.2010.2051036, 2011.

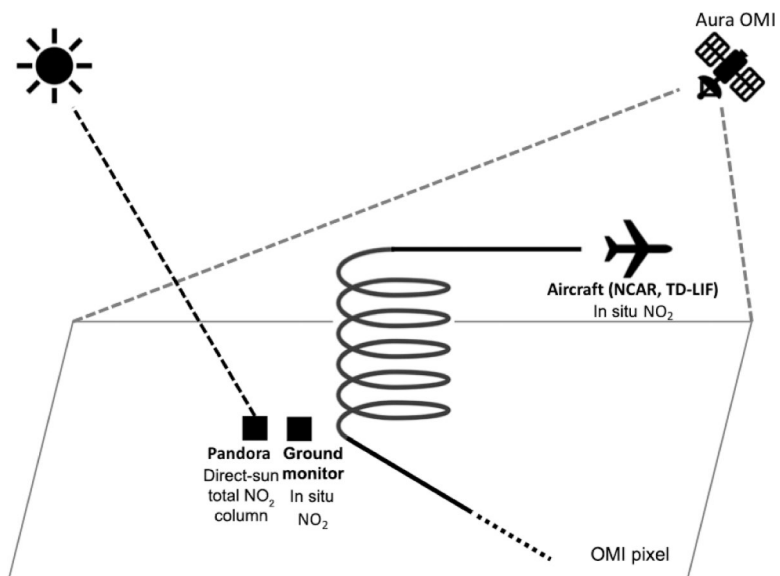


Figure 1. Conceptual illustration of NO₂ observations during the DISCOVER-AQ and KORUS-AQ field campaigns. The instruments used include ground-based monitors measuring in situ NO₂ volume mixing ratios, Pandora making direct-sun measurements to retrieve the total column NO₂, airborne instruments measuring in situ NO₂ profiles, and the Ozone Monitoring Instrument (OMI) aboard the Aura spacecraft reporting total column and tropospheric column NO₂.

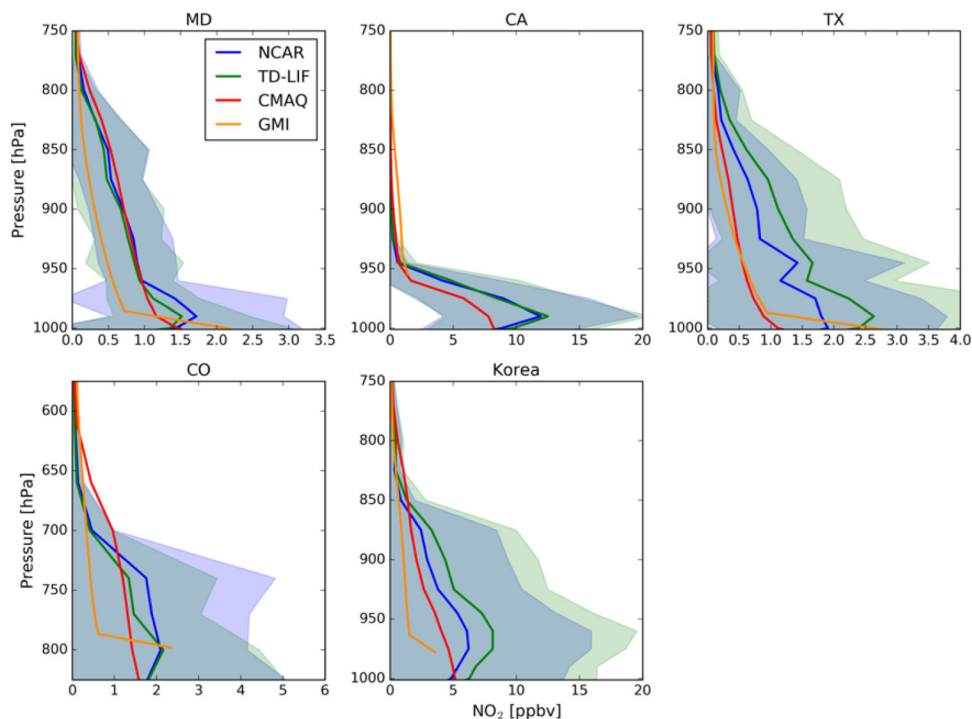


Figure 2. Mean early afternoon NO_2 profiles, both observed and modeled, for the DISCOVER-AQ and KORUS-AQ campaigns. Colored lines represent the average for airborne in situ profiles from NCAR (blue) and TD-LIF (green) instruments compared with simulated profiles from the GMI global model (orange) and the CMAQ (DISCOVER-AQ) or WRF-Chem (KORUS-AQ) regional models (red). The standard deviations of airborne profiles are indicated as shaded areas for NCAR (lavender) and TD-LIF (green) instruments. The blue-gray color represents the overlap of the two.

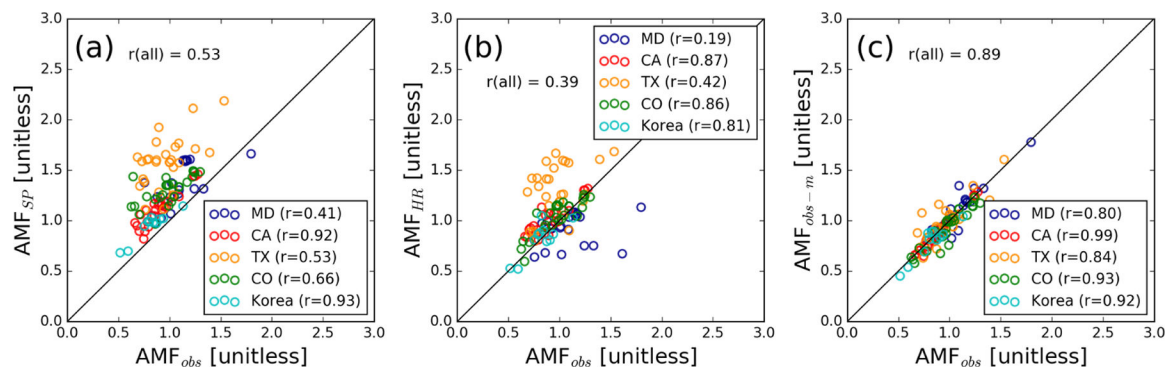


Figure 3.

Comparison of AMFs calculated using observed NO_2 profiles (AMF_{obs}) with tropospheric AMFs in the OMI Standard Product (AMF_{SP} , **a**), and those calculated using NO_2 profiles from high-resolution model simulations (AMF_{HR} , **b**). Panel (**c**) compares tropospheric AMFs using daily versus campaign-average profiles (AMF_{obs-m}). The symbols are color-coded by campaign location.

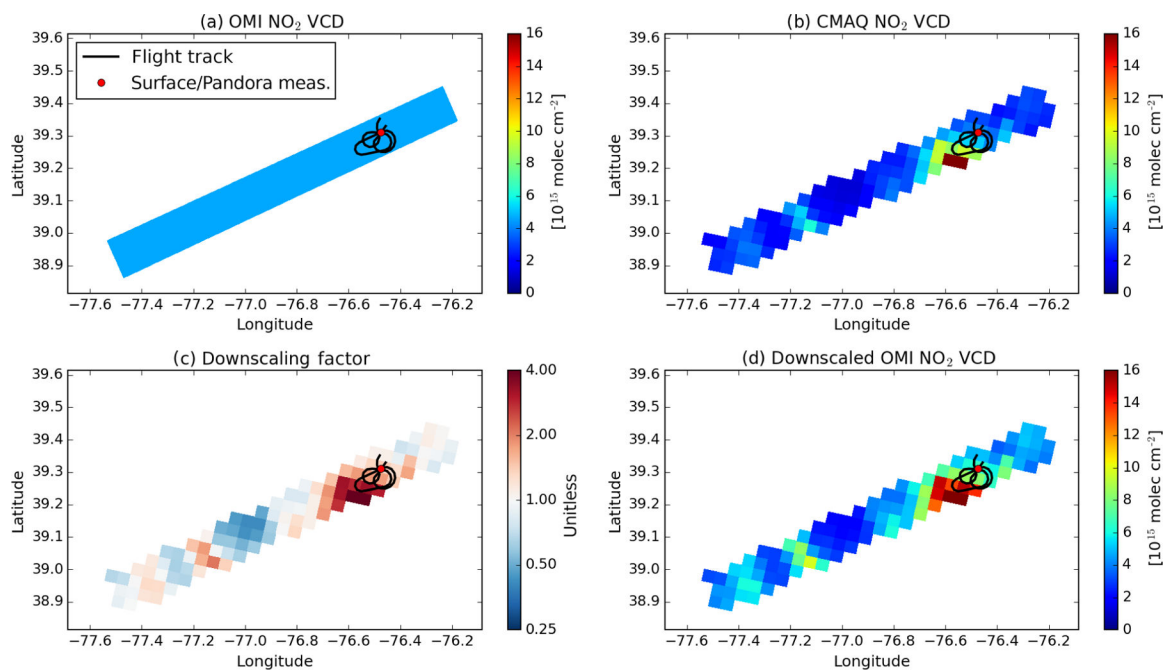


Figure 4.

An illustration of downscaled OMI NO₂ for an OMI pixel over Essex, MD, from orbit 37024 on 1 July 2011. Shown are the original OMI tropospheric NO₂ VCD (a), coincidentally sampled CMAQ NO₂ VCD at a spatial resolution of 4×4 km² (b), the spatial-weighting kernel (c), and downscaled OMI tropospheric NO₂ VCD (d). These pixels coincide with an airborne in situ NO₂ profile sampled during the DISCOVER-AQ Maryland campaign, and the flight route is marked with a black line. The location of the NO₂ surface monitor and Pandora instrument is marked with a red dot.

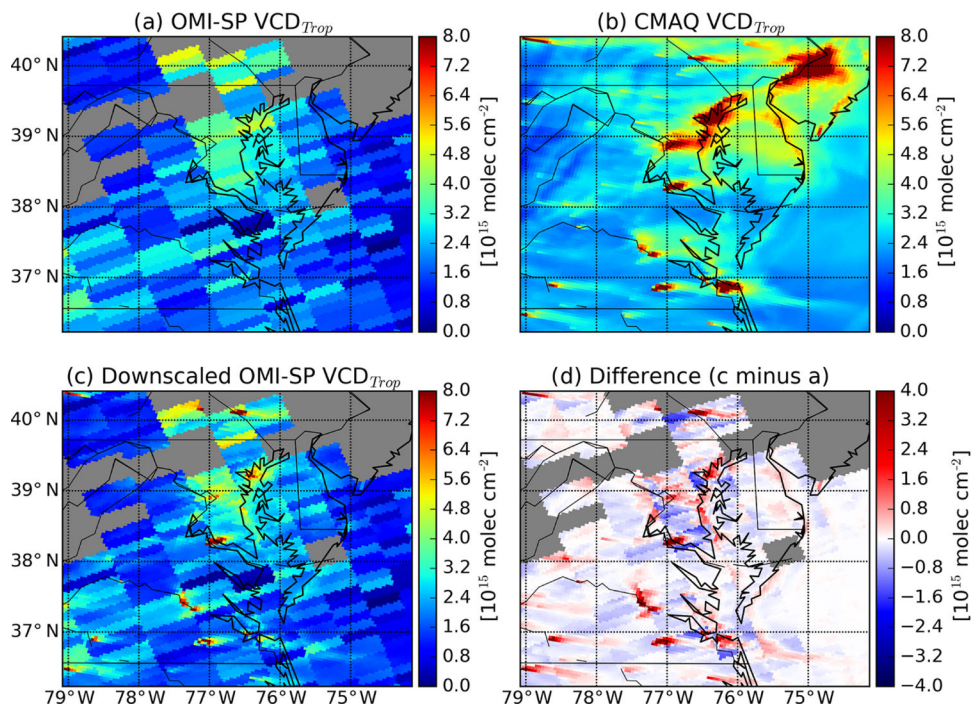


Figure 5. Tropospheric NO₂ VCD maps from (a) OMI SP, (b) CMAQ, and (c) downscaled OMI over Maryland on 29 July 2011. Panel (d) shows the difference between downscaled and standard tropospheric NO₂ VCD data (c minus a). The gray areas represent pixels with an effective cloud fraction > 0.3.

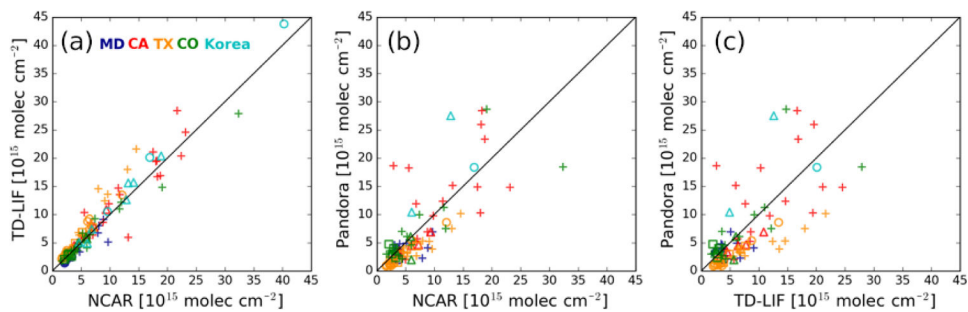


Figure 6. Comparison of NO₂ tropospheric columns derived from NCAR, TD-LIF, and Pandora instruments. Different colors represent the campaign location, and the symbols represent the type of surface monitor (open circle: photolytic converter, plus: molybdenum converter, triangle: CAPS, square: CRDS).

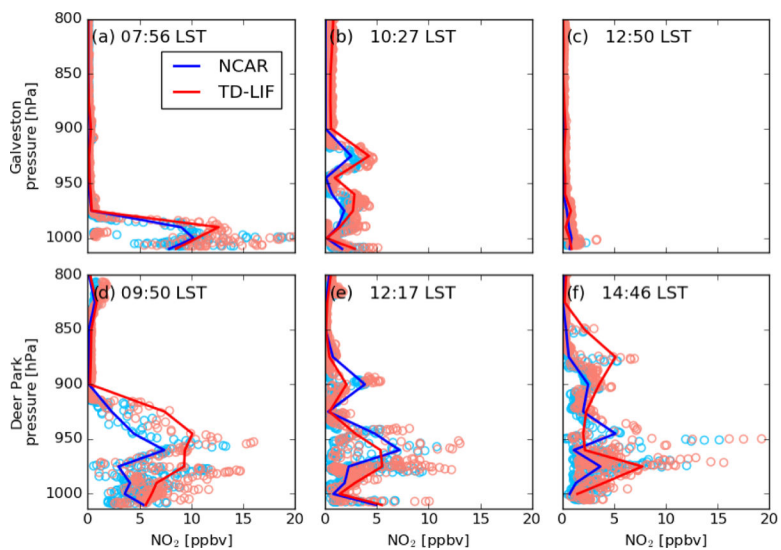


Figure 7. Vertical distribution of NO_2 mixing ratios at different local solar time (LST) over Galveston (a, b, c) and Deer Park (d, e, f) in TX measured by the NCAR (light blue) and TD-LIF (orange) instruments. The circles in lighter colors represent 1 s measurements, and the solid lines show the mean values for NCAR (blue) and TD-LIF (red).

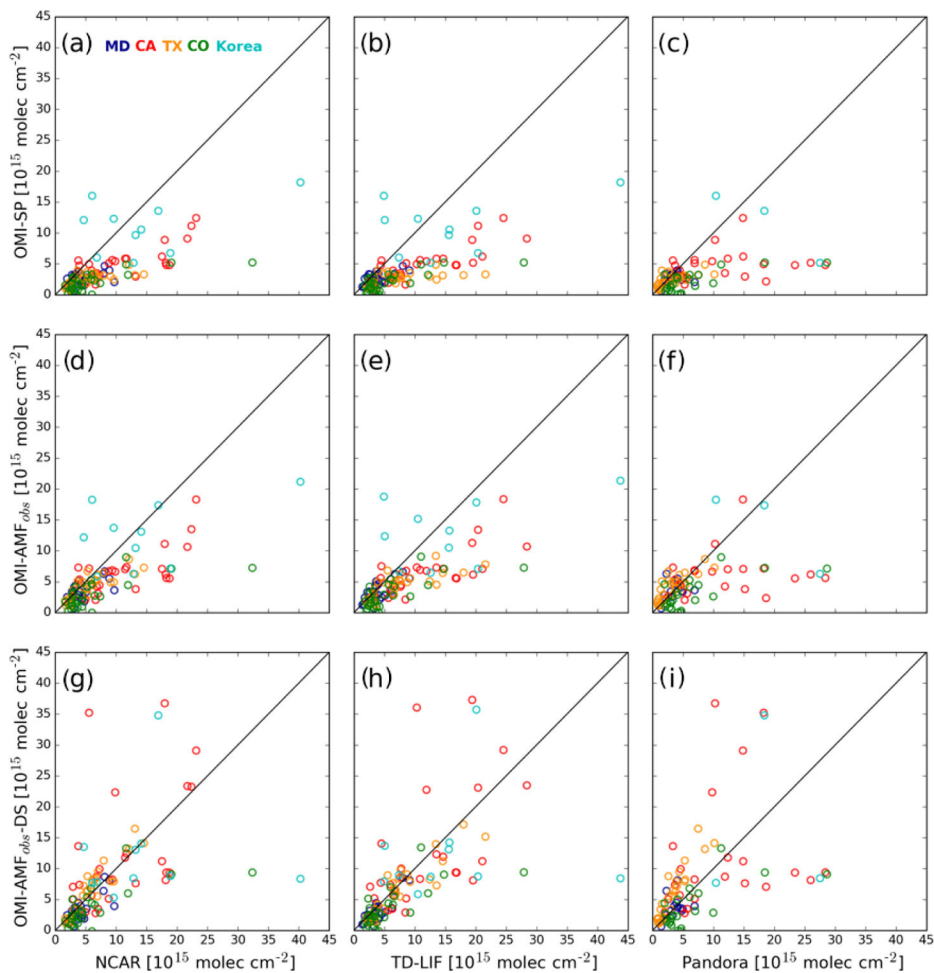


Figure 8. Comparison of tropospheric NO_2 columns from OMI with the data from NCAR (a, d, g), TD-LIF (b, e, h), and Pandora (c, f, i) instruments. OMI retrievals are performed using the default GMI (a–c) and observed NO_2 profiles (d–i). In addition, OMI columns in (g)–(i) are downscaled with high-resolution (CMAQ and/or WRF-Chem) model simulations. Different colors represent the campaign locations.

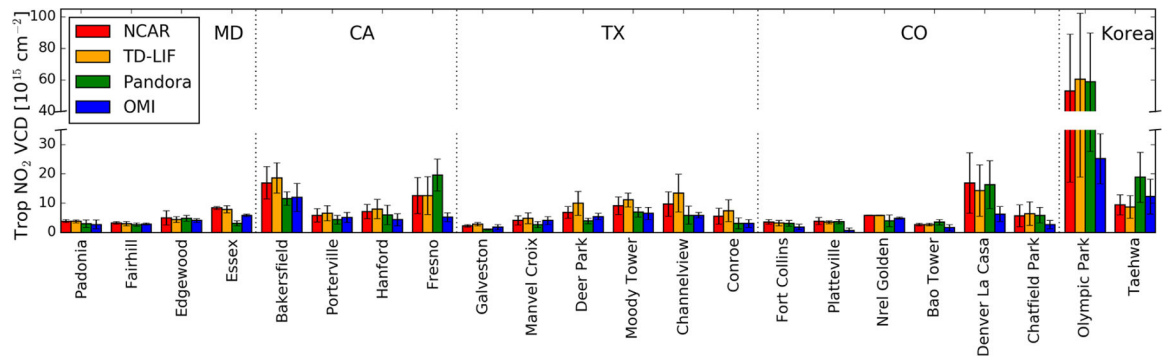


Figure 9. Site mean tropospheric NO₂ VCDs calculated from NCAR (red), TD-LIF (orange), Pandora (green), and OMI (blue). The OMI data are derived using observed NO₂ profiles and downscaled using high-resolution model simulations. The vertical bars represent the standard deviations.

Table 1.

Campaign locations and time periods.

Campaign	Location	Time period	Flight days
DISCOVER-AQ	Baltimore, Maryland	June-July 2011	14
DISCOVER-AQ	San Joaquin Valley, California	January-February 2013	11
DISCOVER-AQ	Houston, Texas	September 2013	10
DISCOVER-AQ	Denver-Ft. Collins, Colorado	July-August 2014	15
KORUS-AQ	Republic of Korea (South Korea)	May-June 2016	22

Table 2.

Summary of ground supersites during DISCOVER-AQ and KORUS-AQ campaigns with ground-based NO₂ measurements. The symbol *N* represents the sample size for aircraft and Pandora (in parentheses if different from that of aircraft profiles) measurements that are collocated with OMI observations. Surface NO₂ monitors include NO_x analyzers with molybdenum converters (MCs), NO_x analyzers with photolytic converters (PCs), cavity-attenuated phase shift (CAPS) spectrometers, and cavity ring-down spectrometers (CRDSs).

Campaign	Site	Latitude, longitude	Elevation (m)	N	Ground monitor type
MD	Padonia	39.46° N, 76.63° W	120	6(4)	PC
	Fairhill	39.7° N, 76.86° W	109	3	PC
	Edgewood	39.4° N, 76.3° W	9	6(5)	PC
	Essex	39.31° N, 76.47° W	13	3(2)	MC
CA	Chesapeake [/]	39.16° N, 76.34° W ²	-	3(0)	-
	Bakersfield	35.33° N, 119.0° W	117	5(3)	MC
	Porterville	36.03° N, 119.06° W	141	5	CAPS
	Hanford	36.32° N, 119.64° W	80	7(6)	MC
	Fresno	36.79° N, 119.77° W	97	8	MC
TX	Galveston	29.25° N, 94.86° W	0	7	PC
	Manvel Croix	29.52° N, 95.39° W	18	6	CRDS
	Deer Park	29.67° N, 95.13° W	6	4	MC
	Moody Tower	29.72° N, 95.34° W	64	4(2)	PC
	Channelview	29.80° N, 95.13° W	6	4	MC
	Conroe	30.35° N, 95.43° W	67	3	MC
	Fort Collins	40.59° N, 105.14° W	1577	3(2)	MC
	Platteville	40.18° N, 104.73° W	1522.5	5(4)	MC
	NREL-Golden	39.74° N, 105.18° W	1846	4(2)	CAPS
	Bao Tower	40.04° N, 105.01° W	1590	4	CRDS
CO	Denver La Casa	39.78° N, 105.01° W	1602	5(4)	MC
	Chatfield Park	39.53° N, 105.07° W	1675	5	MC
	Olympic Park	37.52° N, 127.124° E	26	4(3)	PC
	Taehwa	37.31° N, 127.311° E	160	7(2)	CAPS

[/] Only aircraft spirals were performed over this site.

²The coordinate is approximate.

EPA Author Manuscript

EPA Author Manuscript

EPA Author Manuscript

Table 3.

Comparison between NCAR, TD-LIF, and Pandora NO₂ observations.

Campaign No. of profs. (Pandora)	NCAR vs. TD-LIF		NCAR vs. Pandora		TD-LIF vs. Pandora	
	Mean diff. (%) (TD-LIF - NCAR)	<i>r</i>	Mean diff. (%) (Pandora - NCAR)	<i>r</i>	Mean diff. (%) (Pandora - TD-LIF)	<i>r</i>
MD 21 (14)	-9.6	0.87	-24.5	0.42	-18.3	0.18
CA 25 (22)	7.2	0.93	11.1	0.65	4.8	0.58
TX 28 (26)	31.9	0.97	-39.1	0.94	-53.9	0.93
CO 26 (21)	-6.6	0.99	-2.8	0.81	4.2	0.78
Korea 11 (5)	11.6	0.99	20.3	0.95	7.5	0.94
All 111 (88)	8.3	0.99	-2.0	0.92	-9.8	0.90